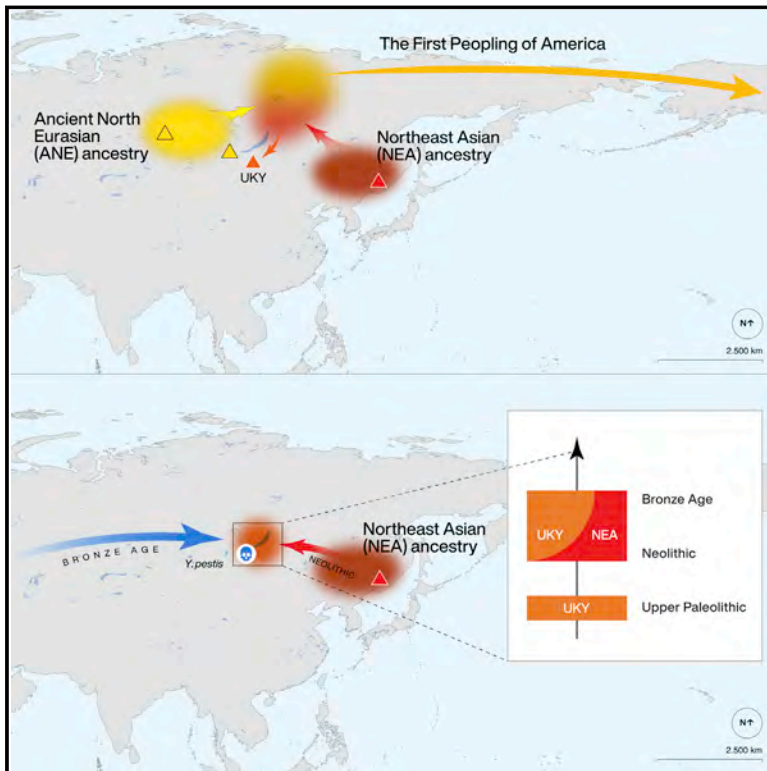# Paleolithic to Bronze Age Siberians Reveal Connections with First Americans and across Eurasia

Graphical Abstract

Authors

He Yu, Maria A. Spyrou,
Marina Karapetian, ..., Cosimo Posth,
Choongwon Jeong, Johannes Krause

Correspondence

posth@shh.mpg.de (C.P.),
jeong@shh.mpg.de (C.J.),
krause@shh.mpg.de (J.K.)

In Brief

Genome-wide ancient DNA data from the Lake Baikal and its surroundings, comprising a time transect of 10,000 years from the Upper Paleolithic to the Early Bronze Age, reveals deeply divergent ancestry that links Upper Paleolithic Siberians and the First Peoples of the Americas and delineates the complex transition between Early Neolithic and Early Bronze Age populations in Siberia.

Highlights

- An Upper Paleolithic Siberian shows a deep link with the First Peoples of the Americas

- A 10,000-year continuum of Ancient North Eurasian ancestry in the Lake Baikal region

- The Neolithic to Bronze Age population formation occurred through prolonged local admixture

- Long-range human and *Y. pestis* mobility across Eurasia during the Early Bronze Age

Cell

CellPress

Article

Paleolithic to Bronze Age Siberians Reveal Connections with First Americans and across Eurasia

He Yu,[1] Maria A. Spyrou,[1] Marina Karapetian,[2] Svetlana Shnaider,[3] Rita Radzevičiūtė,[1] Kathrin Nägele,[1] Gunnar U. Neumann,[1] Sandra Penske,[1] Jana Zech,[4] Mary Lucas,[4] Petrus LeRoux,[5] Patrick Roberts,[4] Galina Pavlenok,[3] Alexandra Buzhilova,[2] Cosimo Posth,[1,6,*] Choongwon Jeong,[1,7,*] and Johannes Krause[1,8,*]

[1]Department of Archaeogenetics, Max Planck Institute for the Science of Human History, Jena 07745, Germany
[2]Research Institute and Museum of Anthropology, Moscow State University, Moscow 125009, Russia
[3]Institute of Archaeology and Ethnography of the Siberian Branch of the Russian Academy of Sciences, Novosibirsk 630090, Russia
[4]Department of Archaeology, Max Planck Institute for the Science of Human History, Jena 07745, Germany
[5]Department of Geological Sciences, University of Cape Town, Rondebosch 7701, South Africa
[6]Institute for Archaeological Sciences, Archaeo- and Palaeogenetics, University of Tübingen, Tübingen 72070, Germany
[7]School of Biological Sciences, Seoul National University, Seoul 08826, Republic of Korea
[8]Lead Contact
*Correspondence: posth@shh.mpg.de (C.P.), jeong@shh.mpg.de (C.J.), krause@shh.mpg.de (J.K.)
https://doi.org/10.1016/j.cell.2020.04.037

SUMMARY

Modern humans have inhabited the Lake Baikal region since the Upper Paleolithic, though the precise history of its peoples over this long time span is still largely unknown. Here, we report genome-wide data from 19 Upper Paleolithic to Early Bronze Age individuals from this Siberian region. An Upper Paleolithic genome shows a direct link with the First Americans by sharing the admixed ancestry that gave rise to all non-Arctic Native Americans. We also demonstrate the formation of Early Neolithic and Bronze Age Baikal populations as the result of prolonged admixture throughout the eighth to sixth millennium BP. Moreover, we detect genetic interactions with western Eurasian steppe populations and reconstruct *Yersinia pestis* genomes from two Early Bronze Age individuals without western Eurasian ancestry. Overall, our study demonstrates the most deeply divergent connection between Upper Paleolithic Siberians and the First Americans and reveals human and pathogen mobility across Eurasia during the Bronze Age.

INTRODUCTION

The Lake Baikal region in Siberia has been inhabited by modern humans since the Upper Paleolithic and has a rich archaeological record (Katzenberg and Weber, 1999; Weber, 1995). In the past 5 years, ancient genomic studies have revealed multiple genetic turnovers and admixture events in this region. The 24,000-year-old individual (MA1) from the Mal'ta site represents an ancestry referred to as "Ancient North Eurasian (ANE)," which was widespread across Siberia during the Paleolithic (Fu et al., 2016; Raghavan et al., 2014a; Sikora et al., 2019) and that contributed to the genetic profile of a vast number of present-day Eurasian populations as well as Native Americans (Haak et al., 2015; Lazaridis et al., 2014, 2016; Raghavan et al., 2015). ANE ancestry was suggested to have been largely replaced in the Lake Baikal region during the Early Neolithic by a gene pool related to present-day northeast Asians, with a limited resurgence of ANE ancestry by the Early Bronze Age (Damgaard et al., 2018a).

Siberia has also been proposed as a source for multiple waves of dispersals into the Americas, the first of which was shown to be driven by a founding population estimated to have formed around 25,000–20,000 years before the present (BP) (Raghavan et al., 2015). The so-called Ancient Beringian ancestry represented by a 11,500-year-old Alaskan individual (USR1) was shown to be part of this founding population, estimated to have split from other Native Americans around 23,000 BP (Moreno-Mayar et al., 2018). In addition, the recently published 9,800-year-old Kolyma genome from northeastern Siberia was suggested to represent the closest relative to Native American populations outside of the Americas (Sikora et al., 2019). Moreover, the Paleo-Eskimo ancestry represented by a 4,000-year-old Saqqaq individual from Greenland was also estimated to have split from northeastern Siberian groups and migrated to Arctic America around 6,000–5,000 BP (Flegontov et al., 2019; Raghavan et al., 2014b; Rasmussen et al., 2010). Although these waves of migration are generally linked to ancient Siberian populations, their origins in the context of the Siberian genetic history remain poorly understood. Further studies of the Siberian population history using ancient genomes are, therefore, critical for the better understanding of the formation of Native American populations.

Furthermore, the Neolithic to Bronze Age transition in Eurasia was marked by complex cultural and genetic changes facilitated by extensive population movements, though their impact in the Lake Baikal region is still unclear. Looking to the west, the Early Bronze Age groups from the Pontic-Caspian steppe associated with the Yamnaya complex spread both east and west along with their distinct genetic profile often referred to as "Steppe ancestry" (Allentoft et al., 2015; Haak et al., 2015). The eastward expansion of this group is considered to be associated with the Early Bronze Age Afanasievo culture. However, the later Middle Bronze Age Okunevo-related population from the central steppe as well as the Late Bronze Age Khövsgöl-related population from the eastern steppe harbor only a limited proportion of Steppe ancestry (Jeong et al., 2018, 2019). Therefore, the effect of steppe migrations in eastern Eurasia, particularly the interactions of Bronze Age Baikal hunter-gatherers with the contemporaneous and geographically proximal Afanasievo population, is still largely unexplored.

In this study, we report 19 newly sequenced ancient hunter-gatherers from the Lake Baikal and its surrounding regions, spanning from the Upper Paleolithic to the Early Bronze Age. Their analyses alongside published data reveal the most deeply divergent ancestry that link Upper Paleolithic Siberians and the First Peoples of the Americas, and more clearly delineate the complex transition between Early Neolithic and Early Bronze Age populations in the Lake Baikal region. We also provide both human and pathogen genomic evidence demonstrating the influence of western Eurasian steppe populations in this region during the Early Bronze Age and discuss the genetic contribution of Lake Baikal hunter-gatherers to Siberian populations through time.

RESULTS

Ancient DNA Sequencing
We generated genome-wide genotype data from 19 ancient humans, including one Upper Paleolithic individual (dated to 14,050–13,770 BP, see Orlova, 1995; Pavlenok et al., 2019), four Early Neolithic individuals (7,320–6,500 BP), and 14 Late Neolithic to Early Bronze Age (LNBA) individuals (4,830–3,570 BP) from a total of 10 archaeological sites (Figure 1; Table S1). The radiocarbon date offsets caused by the local freshwater reservoir were estimated using the carbon and nitrogen isotopic values as described in previous studies on the same region (see STAR Methods; Schulting et al., 2014, 2015). We built single- and double-stranded DNA libraries from teeth or petrous portions of the temporal bone for the studied individuals, and shotgun sequencing revealed high levels of DNA preservation with endogenous DNA contents ranging from 0.12% to 50.54% (Table S1). Subsequently, libraries were enriched for human DNA by SNP-capture targeting a set of 1.24 million variable sites (Fu et al., 2015) and sequenced to mean coverage ranging from 0.04X to 2.07X. Pseudo-haploid genotypes were called on the targeted SNPs by randomly sampling a single allele at each position, with 34k to 886k SNPs covered by our samples. Additionally, we performed deep shotgun sequencing on eight individuals with high endogenous DNA levels (12%–51%), to achieve genomic coverage that ranged from 0.1X to 1.9X and refined

their diploid genotypes by genotype likelihood-based imputation, resulting in 386k to 518k SNPs overlapping with the *Human Origins* dataset (Table S1).

We determined genetic sex by comparing the coverage on the sex chromosomes with the autosomal chromosomes, which revealed four females and 15 males. All individuals revealed low modern human DNA contamination at the mitochondrial level as well as through an estimation of X chromosomal heterozygosity on male individuals, except for KAG001 that showed 9.6% nuclear contamination (Table S1). No kin relationship was found among these individuals. We finally intersected our genotypes with SNPs on the Affymetrix *Human Origins* array (Lazaridis et al., 2014) and combined with published genotype data from 3,014 present-day worldwide individuals and 453 ancient individuals for population genomic analysis (Table S1).

Population Structure
We first performed principal-component analysis (PCA) to understand the genetic background of the studied individuals, against modern Eurasian and Native American populations, and projected selected ancient individuals onto the PCs calculated with modern ones (Figure 1C). Most of the Lake Baikal individuals occupied the space on a "ANE-NEA" cline running between "Northeast Asian" (NEA) ancestry represented by Neolithic hunter-gathers from the Devil's Gate in the Russian Far East (Sikora et al., 2019; Siska et al., 2017), and the ANE ancestry represented by Upper Paleolithic Siberian individuals MA1, AfontovaGora 2 (AG2), and AfontovaGora 3 (AG3) (Fu et al., 2016; Raghavan et al., 2014a), which was first described by Damgaard et al. (2018a). Our newly sequenced Upper Paleolithic genome from the Ust-Kyakhta-3 site (UKY) just south to the Lake Baikal is placed close to the Mesolithic northeastern Siberian Kolyma individual (Sikora et al., 2019) and is shifted toward Native American populations compared to the rest of the ancient Baikal individuals along PC2. All four Early Neolithic individuals cluster with published Early Neolithic groups from the same region (Shamanka_EN, Lokomotiv_EN, UstBelaya_EN) (Damgaard et al., 2018a; Flegontov et al., 2019) designated as the "Baikal_EN" population. The LNBA individuals were divided into four groups. The major "Baikal_LNBA" group included 10 individuals and clustered with published Late Neolithic to Bronze Age Baikal populations (Shamanka_EBA, Kurma_EBA, UstIda_EBA, UstIda_LN, UstBelaya_BA). These individuals were positioned in PCA closer to ANE-related individuals compared with the Early Neolithic individuals from the same region, as well as closer to the Paleo-Eskimo Saqqaq individual (Rasmussen et al., 2010). Another two individuals (GLZ001 and GLZ002) from the Glazkovskoe predmestie site, unlike the third individual from the same archaeological site (GLZ003), seemed shifted from the main cluster and showed closer genetic affinity to the Devil's Gate and Early Neolithic Baikal individuals. One of the six individuals from the Kachug site (KPT005) was substantially displaced from the Baikal_LNBA group toward western Eurasians along PC1, not along the ANE-NEA cline but toward later Bronze Age populations, suggesting a potential introgression of the Steppe-related ancestry. Finally, an Early Bronze Age individual (BZK002) from the Bazaikha site in the Yenisei River region further to the west of the Lake Baikal was significantly displaced
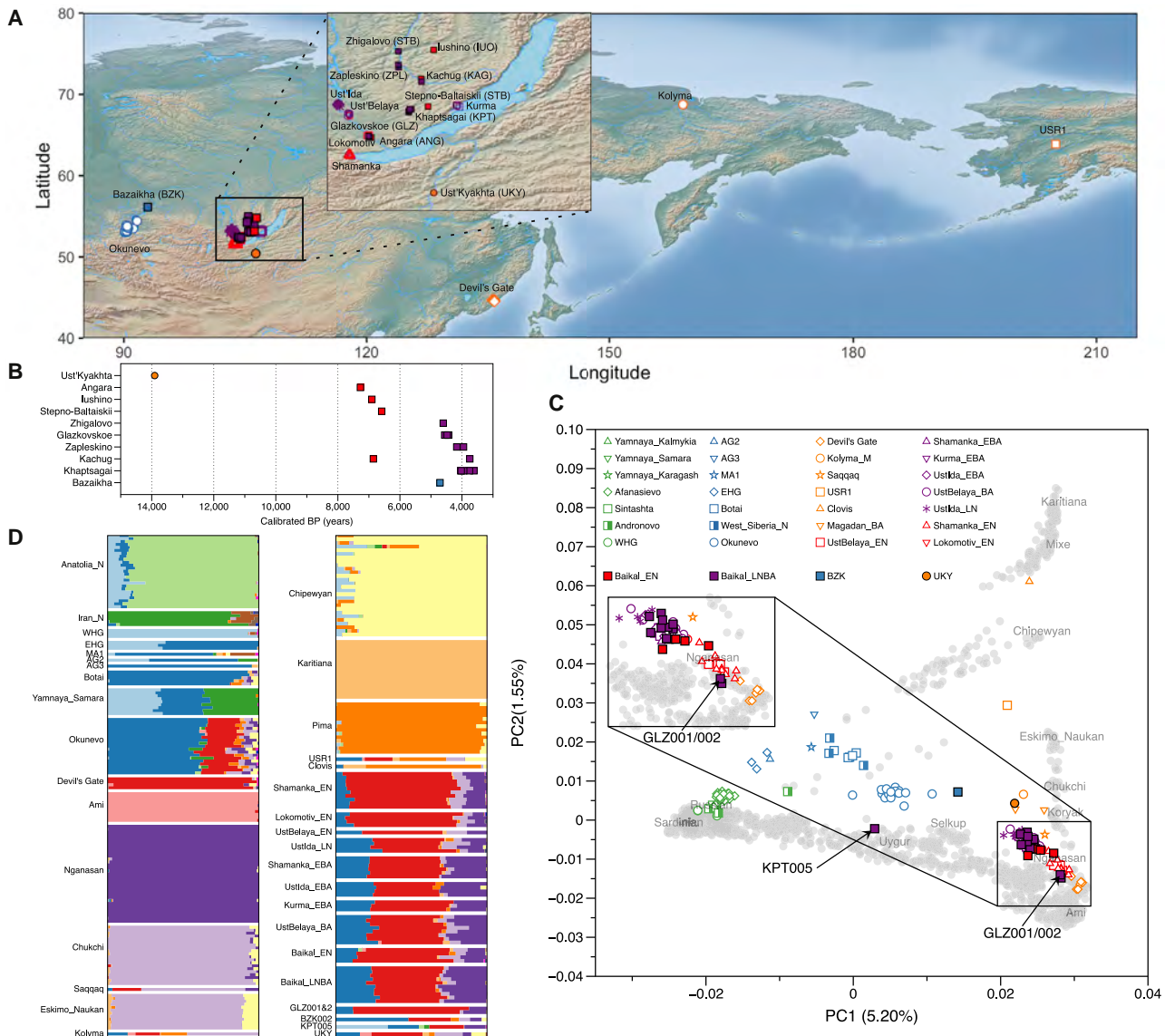
Cell
Article

CellPress

Figure 1. Geographic Location, Time Period, and Genetic Profile of Studied Individuals

(A) Location of the 19 newly reported and published ancient individuals relevant in this study. Newly reported individuals are shown in outlined squares or circles.

(B) Ages of newly reported individuals from each site, with the x axis showing the median calibrated radiocarbon dates after correction for freshwater reservoir effect.

(C) PCA of Eurasian and Native American populations. The modern individuals are shown in light gray circles, with the name of several representative populations marking the positions of West Eurasians (Sardinian), East Asians (Ami and Uyghur), Siberians (Chukchi, Eskimo Naukan, Koryak, Nganasan, Selkup), and Native Americans (Chipewyan, Mixe, Karitiana). Ancient individuals are shown in colored symbols. The individual KPT005, which showed a significant shift toward west Eurasian populations, and individuals GLZ001&GLZ002, which also represented outlier genetic profiles, are marked out with an arrow.

(D) Population clustering pattern of studied individuals together with representative modern and ancient populations, when K = 16. Most Early Neolithic to Bronze Age Lake Baikal region individuals are modeled as admixture of northeast Asian (dark red), ANE (dark blue), and Nganasan component (purple). The BZK002 individual has similar genetic profile as Okunevo, with a significantly larger ANE proportion compared with Baikal individuals, while the KPT005 individual shows a large component associated with WHG (light blue).

See also Figure S1 and Table S1.

toward ANE-related individuals and located close to published Bronze Age individuals associated to the Okunevo culture (Damgaard et al., 2018a).

Population clustering with ADMIXTURE based on worldwide populations also showed a similar clustering pattern. When

selecting a K value of 16 (see STAR Methods), the published and newly sequenced individuals belonging to main Early Neolithic to Bronze Age Baikal groups all showed genetic profiles composed of a mixture of three major components that were mostly enriched in ANE-related individuals, northeast

Asians, and central Siberians represented by the Uralic-speaking Nganasan population (Figure 1D). The ANE and central Siberian ancestries were both of higher proportion in most LNBA Baikal individuals than in the Early Neolithic ones, while GLZ001 and GLZ002 showed higher NEA ancestry, similar to the Early Neolithic population. The BZK002 individual presented a profile similar to the published Okunevo group (Damgaard et al., 2018b), with a much larger ANE component compared to other Lake Baikal individuals. The KPT005 individual also displayed a substantial contribution derived from European "Western Hunter-Gatherer" (WHG) ancestry, likely acquired through gene flow from the west.

We estimated the runs of homozygosity (ROH) of selected individuals together with published Baikal individuals (Table S1) and did not identify an inbreeding signal in any individual. The Kolyma individual showed significantly more ROH compared with other individuals, suggesting a smaller population size in Mesolithic northeastern Siberia (Figure S1). The sharing of identity-by-descent (IBD) segments between individuals suggested a close relationship between UKY and Kolyma, supporting our analyses based on genome-wide SNP data, and also revealed that Early Neolithic and LNBA Baikal individuals shared genetic affinity with each other as well as with the older UKY and Kolyma genomes (Figure S1).

Upper Paleolithic Baikal Ancestry Links with Non-Arctic Native Americans

In the population structure analysis, we found the Upper Paleolithic UKY individual to be closely related with the northeastern Siberian Kolyma individual. This is further validated by outgroup f_3 statistics (Figure 2A) where, similarly to Kolyma, UKY showed close genetic affinity with Native American and Beringian populations (Figure 2A). F_4 statistics in the form of f_4(Mbuti, X; Kolyma, UKY) revealed that Kolyma is more closely related to populations from northeastern Siberia and North America compared with UKY (Figure S2). We further applied f_4 statistics to explore the relationship of UKY and Kolyma with Native Americans and USR1 that was described as an outgroup to all non-Arctic Native Americans (Moreno-Mayar et al., 2018). Both UKY and Kolyma were symmetrically related with non-Arctic Native Americans and USR1, while USR1 shared significantly more genetic affinity with Native American populations compared to UKY and Kolyma (Figure S2; Table S2).

We also investigated their genetic composition using *qpAdm* modeling (Haak et al., 2015) and found that both UKY and Kolyma possessed a similar level of ANE contribution, around 30%, when modeled as two-way mixture of Devil's Gate (representing NEA ancestry) and AG3 (representing ANE ancestry) (Table S3). Noticeably, this model did not fit well for both UKY (p = 1.45E-03) and Kolyma (p = 3.98E-08), as the Native American Karitiana population showed extra affinity with the tested individuals compared to the fitted model (Table S3). This observation suggests that UKY and Kolyma shared a certain degree of genetic drift with Native American populations that occurred after the ancestors of Native Americans diverged from ANE and NEA ancestries.

We further explored the relationships among UKY, Kolyma, and ancient Native American groups using the graphic-based

qpGraph modeling (Patterson et al., 2012; Reich et al., 2009). We found that both UKY and Kolyma could be modeled as mixture between a northeast Asian lineage and a sister group of the Native American clade represented by USR1, Ancient Southwestern Ontario (ASO) individuals from Canada, and Early San Nicolas (ESN) individuals from the California Channel Islands in the USA (Scheib et al., 2018; Figure S2). When UKY and Kolyma were included in the same graph, they were consistently modeled as descendants from two independent admixture events, with ancestral lineages of both deriving from the Native American-related and the northeast Asian-related clades (Figure 2B). These findings confirm the close affinity of UKY and Kolyma to Native Americans but also highlight that both lineages contributing to UKY were ancestral to the groups contributing to Kolyma. In addition, aside from the first wave migrating into the Americas through Beringia, the admixture modeling suggests that the source of the Native American ancestry was more broadly spread across Siberia during the Upper Paleolithic, as UKY was found to be ~4,000 years older and over 3,000 km further to the southwest from Kolyma. In fact, our admixture graph indicates that this basal Native American group experienced multiple genetic contacts with northeast Asian populations giving rise to distinct ancient Siberian populations.

Complex Transition between the Early Neolithic and Bronze Age in the Lake Baikal Region

A previous study described the transition between Early Neolithic and Bronze Age populations from the Lake Baikal region as the result of a discrete admixture event of ANE ancestry into the local gene pool (Damgaard et al., 2018a). In this study, we combined the newly sequenced Baikal_EN and Baikal_LNBA individuals with published data from the same time period (Figure 1C) and analyze these two combined datasets, Baikal_EN_all (n = 19) and Baikal_LNBA_all (n = 34), to better elucidate the genetic transition that occurred in this region. Prior to analyzing the combined groups, we confirmed the similarity between the new individuals and published groups using outgroup f_3 statistics. Both Baikal_EN and Baikal_LNBA groups showed the highest genetic affinity with published Early Neolithic and LNBA Baikal populations, respectively (Table S4).

From outgroup f_3 statistics of the combined groups, we found both of the Baikal Early Neolithic and LNBA groups to be sharing high genetic affinity with ancient and modern northeast Asian and Siberian populations (Figure S3). The LNBA Baikal population also showed a high genetic affinity with the Paleo-Eskimo Saqqaq individual. Compared to their NEA proxy, they both carried extra genetic affinity with ANE-related populations while the LNBA population more so than the Early Neolithic population, as shown by f_4 statistics (Figure S3). These results revealed the existence of ANE-related ancestry in the Early Neolithic population and, at the same time, validated the previous finding that an extra ANE ancestry gene flow is responsible for the genetic shift between Early Neolithic and Bronze Age Baikal populations.

We further applied *qpAdm* modeling to quantify the proportion of ANE-related ancestry in Early Neolithic and LNBA Baikal populations, Saqqaq and Nganasan. Using Devil's Gate as the NEA proxy, the Upper Paleolithic UKY was found to be a better fit than Kolyma as the ANE-related proxy for both Baikal populations,
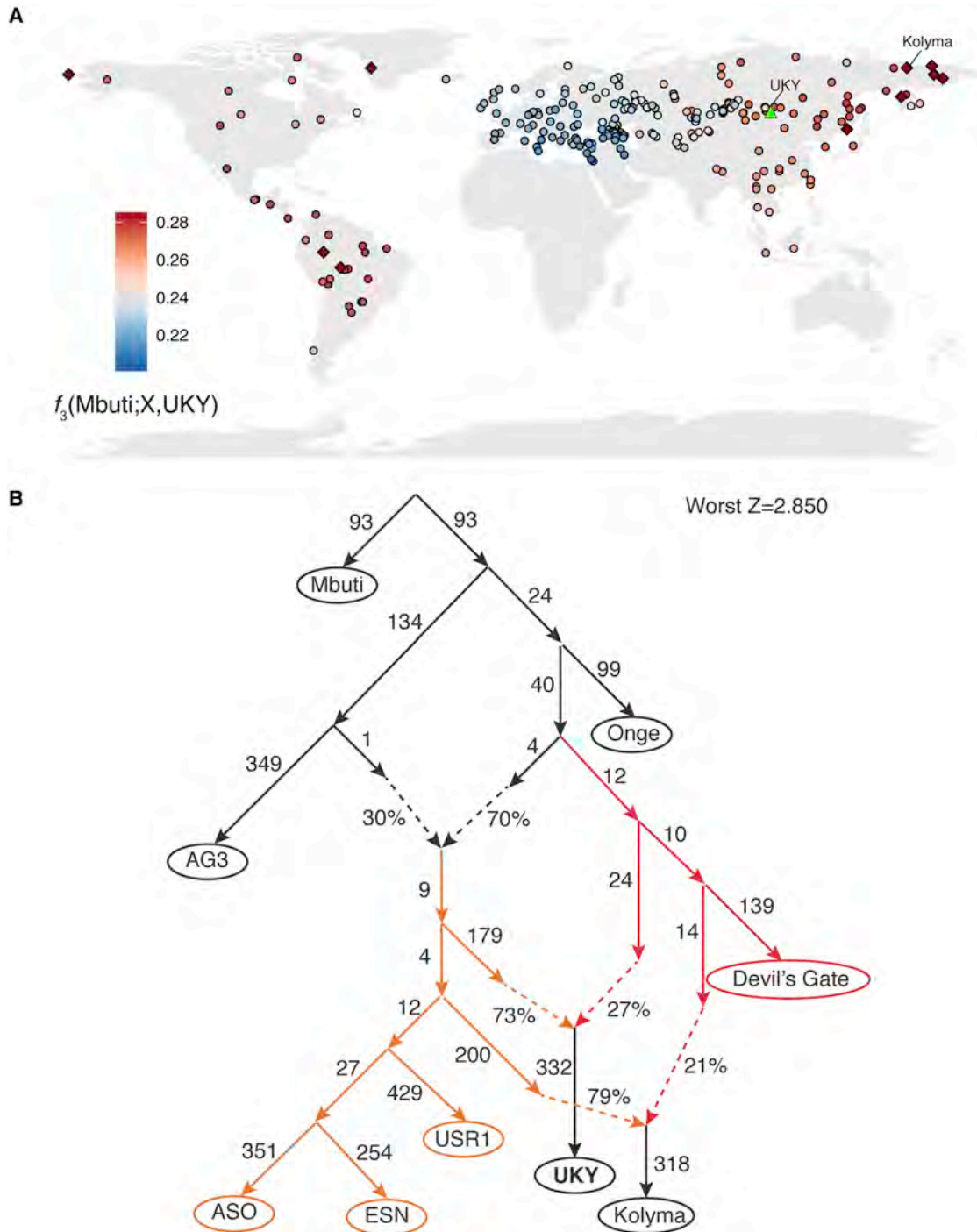
Cell
Article

CellPress

Figure 2. Genetic Affinity between Upper Paleolithic UKY, Kolyma, and Native Americans

(A) Genetic affinity between UKY and worldwide population assessed by f_3(Mbuti;X,UKY). The sampling location of UKY is shown with a green triangle. The 10 test populations with highest f_3 values are shown in diamonds and other populations in circles.

(B) Graphic model of the relationship among UKY, Kolyma, and Native American populations. We first find the best fitted model with only UKY or only Kolyma as described in Figure S2 and then add Kolyma on the selected model with UKY and choose the best model based on maximum f-statistics Z scores and final scores reported for each model. The lineages related with Native American population are colored orange, and the northeast Asian-related lineages are colored red.
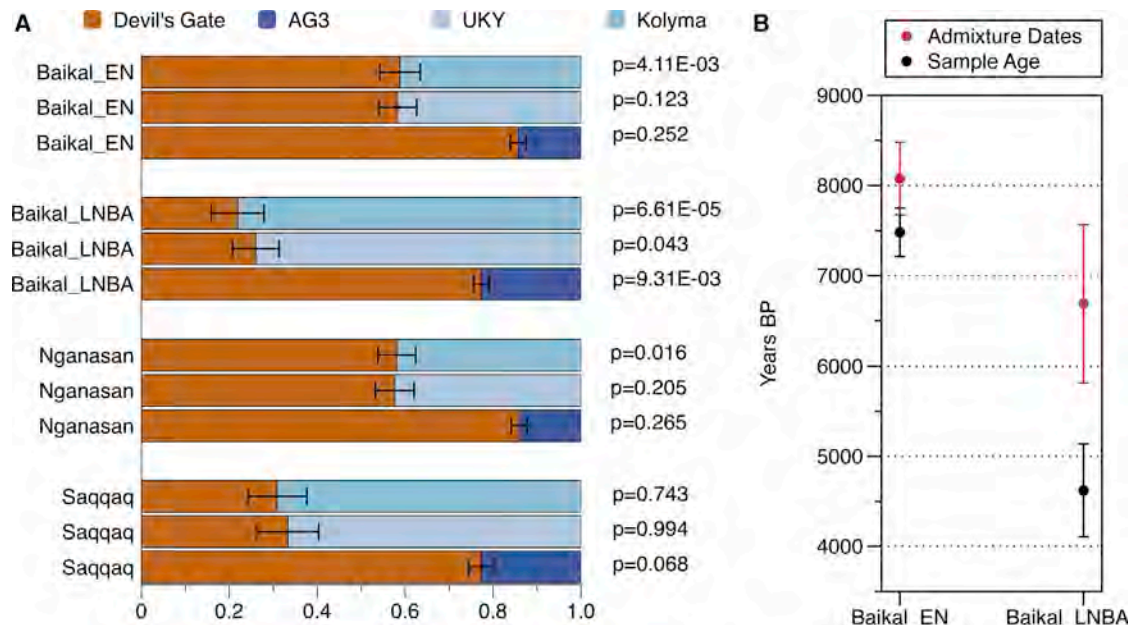
See also Figure S2 and Table S2.

Figure 3. Genetic Modeling of Early Neolithic to Bronze Age Baikal Individuals and Admixture Dating

(A) *qpAdm* modeling of Early Neolithic and LNBA Baikal populations, together with Nganasan and Saqqaq, as admixture between NEA ancestry represented by Devil's Gate and different ANE ancestries. The error bars show the standard errors of estimated ancestry proportions. Details for the modeling are provided in Table S3.

(B) Estimated dates of admixture events between ANE and NEA ancestries in Early Neolithic and LNBA Baikal population. The individual ages are the averages and standard deviations of median radiocarbon dates without correcting for freshwater reservoir effect, to be consistent with previously published individuals. The estimated admixture dates are calculated with generation time of 29 years, and the error bars show the sum of standard errors of DATES estimations and individual ages.

See also Figures S3 and S4 and Tables S3, S4, and S5.

while AG3 provided a good fit for the Early Neolithic population (Table S5). Using Devil's Gate and AG3 as the two proxies of NEA and ANE ancestries, respectively, we estimated the ANE-related ancestry increasing from 14.3% in the Early Neolithic Baikal population to 22.7% in the LNBA population (Figure 3A; Table S3). Of note, the northeastern Siberian Kolyma individual could work as a sufficient ANE proxy for Saqqaq, as described in the study where this genome was first reported (Sikora et al., 2019) but did not provide a good fit for the Baikal populations and Nganasan. This suggests that the Baikal hunter-gatherer and Nganasan populations are more likely to have formed in central or southern Siberia while Paleo-Eskimo ancestry could have emerged in either central or northeastern Siberia.

Furthermore, the program *DATES* was used to date the admixture events between ANE and NEA ancestries in the Baikal population based on the decay of ancestry covariance (Moorjani and Patterson, 2018). We detected a recent admixture signal in the Early Neolithic population, estimated to around 21 generations ago, while the admixture signal in LNBA population was dated to 71 generations ago, although this group harbored significantly more ANE-related ancestry (Table S5). When considering the average radiocarbon date of each population and the standard errors of their admixture dates, we identified contiguous intervals for the admixture events that spanned ∼8,500–6,000 BP, considering a generation time of 29 years (Figure 3B; Figure S4; Table S1; Table S5). Assuming a dating offset of 400–500 years due to freshwater reservoir effect estimated for the newly re-

ported individuals, the admixture timings ranged between ∼8,000 and 5,500 BP. This suggests that both Baikal populations could have been formed through an extended admixture process between local groups and northeast Asian-related populations. The Early Neolithic groups were thus found to have experienced a prolonged admixture process, in contrast to the discrete and rather abrupt event suggested earlier (Damgaard et al., 2018a). This admixture, however, did not continue substantially in the Late Neolithic and Bronze Age, as suggested by the older admixture date for the LNBA population (Figure 3B) and the relatively larger genetic variation among Early Neolithic individuals compared to the homogeneous LNBA cluster, as shown in the PCA plot (Figure 1C).

High Mobility in Bronze Age Siberia Revealed by Genetic Outliers

Among the LNBA Baikal individuals, we identified three outlier individuals, which showed distinct genetic backgrounds from the major group. The genetic profile of the KPT005 individual suggested its affinity to western Eurasian populations inferred from PCA and ADMIXTURE results (Figure 1). Using *qpAdm* modeling, we found that this individual could indeed be modeled as the mixture between the LNBA Baikal and multiple Bronze Age western steppe populations, with the Steppe ancestry contribution ranging between 42% and 48% (Figure 4A; Table S5). Considering geography and radiocarbon dates, we suggest the most likely candidate in our dataset for the source of
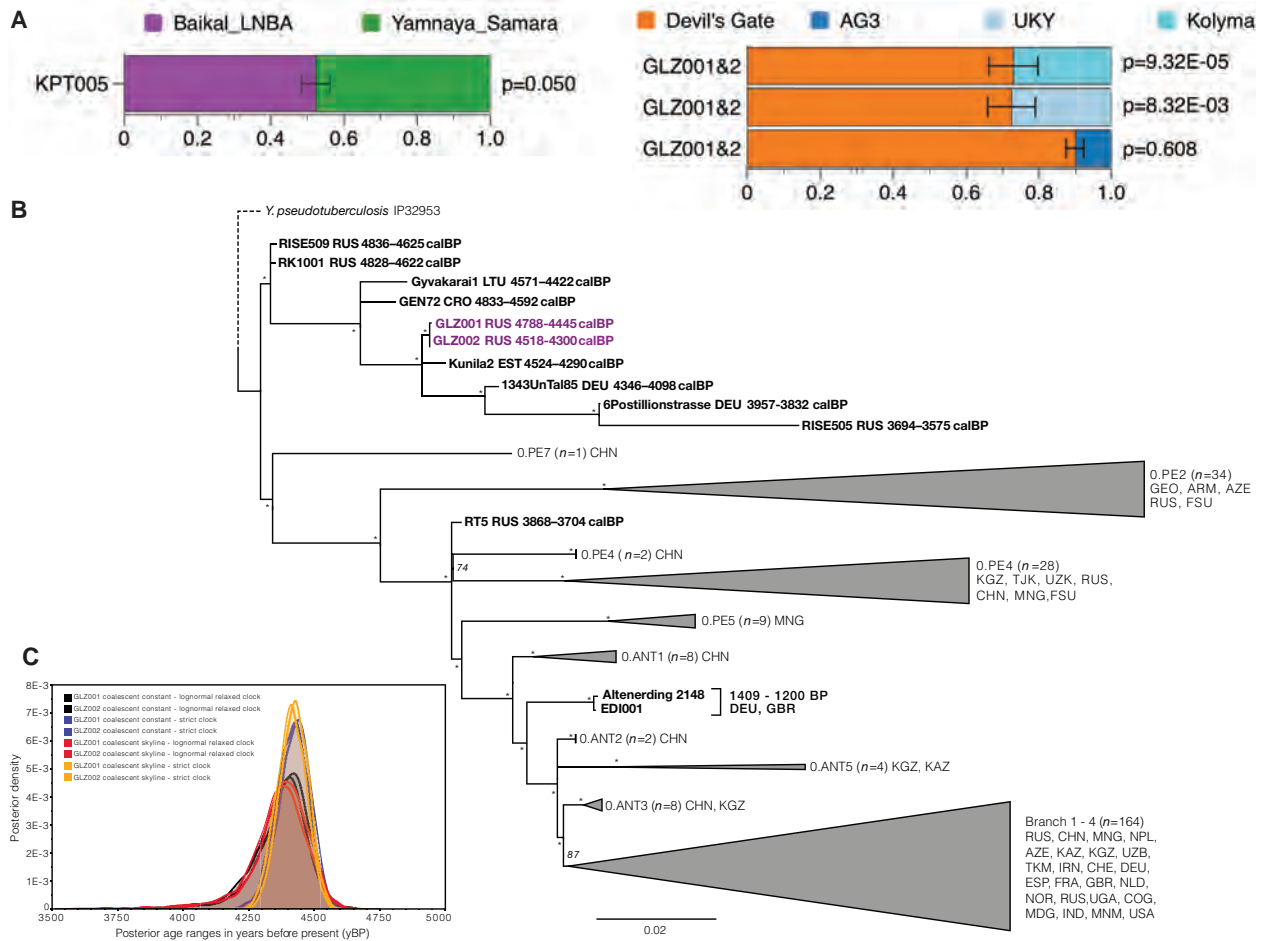
CellPress

Figure 4. Modeling of Genetic Outliers and the *Yersinia pestis* Phylogeny

(A) *qpAdm* modeling of KPT005 as admixture between LNBA Baikal and steppe populations and GLZ001&GLZ002 as admixture between different ANE ancestries and NEA. The error bars show the standard errors of estimated ancestry proportions. Details of the modeling are provided in Table S3.

(B) Maximum likelihood phylogeny of *Y. pestis* genomes based on 4,368 SNPs, generated by applying a 99% partial deletion on the full SNP alignment. The newly reconstructed GLZ001 and GLZ002 genomes are analyzed alongside nine previously published Late Neolithic and Bronze Age genomes, two 6th century genomes from modern-day Germany and England associated with the first plague pandemic and a set of 14th-to-18th-century genomes from the second plague pandemic (ancient comparative dataset n = 28). In addition, they are analyzed alongside a worldwide modern dataset of 233 *Y. pestis* isolates (see full list; Keller et al., 2019). Branches of modern-day isolates were collapsed to enhance tree clarity. Nodes with ≥95 bootstrap support are indicated by asterisks (*). Scale denotes substitutions per site.

(C) Overlapping posterior distributions of the Bayesian age estimates for GLZ001 and GLZ002, determined using BEAST v1.8. The median estimates for all tested models and their accompanying highest posterior densities (95%) are shown in Table S6.

See also Figures S5 and S6 and Tables S3 and S6.

admixture to be the Yamnaya-related Afanasievo population from nearby Altai-Sayan region.

Additionally, we also identified two Early Bronze Age Baikal individuals (GLZ001 and GLZ002) showing significantly lower ANE admixture levels compared to the major Baikal_LNBA group (Figure 1C). We estimated the ANE contribution in these two individuals to be around 10%, using Devil's Gate and AG3 as proxies of NEA and ANE ancestries, respectively (Figure 4A; Table S3). Furthermore, these two individuals both carried Y chromosome haplogroup C2b1, which was predominant in Early Neolithic Baikal populations (Table S1), while the other LNBA individuals carried exclusively Q1a haplogroup. This could indicate either a relic population with ANE ancestry proportion

similar to, or even less than, the Early Neolithic population preserved until the Bronze Age, or immigrants from surrounding regions carrying more NEA ancestry.

The mobility of the Baikal individuals during their lifetimes was thus investigated through the application of strontium isotope analysis to the enamel of eleven teeth samples (Bentley et al., 2004; Price et al., 2002). We found that ten out of the eleven individuals all had values within the bioavailable ^{87}Sr/^{86}Sr range (~0.708–0.711) comprehensively reported for the Baikal region (Haverkort et al., 2010). By contrast, GLZ001 had a ^{87}Sr/^{86}Sr value >0.713 that suggested a non-local origin for this individual, followed by movement to the Angara River Valley region after the period of formation of the second molar (>7 years of age)

(Alexander Bentley, 2006). Based on existing bioavailable strontium data, sources of origin plausibly include areas to the south and east of Lake Baikal on Archean and Proterozoic geology (Haverkort et al., 2010). GLZ002 appears instead "local" to the Angara River Valley in terms of $^{87}Sr/^{86}Sr$, despite the genetic similarity to individual GLZ001. Though a speculation, it is possible that GLZ002 could have migrated to the region during childhood, prior to 7 years of age and, hence, prior to the formation of the second molar, or from a region with similar $^{87}Sr/^{86}Sr$ range to the Angara River Valley.

Identification of *Y. pestis* Infections among Genetic Outlier Individuals

Recent studies have reported evidence of *Yersinia pestis* infections in humans across multiple regions of Europe and central Asia between the Middle Neolithic and Bronze Age (~4,900–3,500 BP) (Andrades Valtueña et al., 2017; Rascovan et al., 2019; Rasmussen et al., 2015b; Spyrou et al., 2018). To date, the majority of identified strains group on an extinct phylogenetic lineage previously designated as the LNBA lineage (Andrades Valtueña et al., 2017). Such data have been interpreted alongside human population genetic frameworks, suggesting the spread of this lineage via Yamnaya-related human migrations across Eurasia during the Late Neolithic and Early Bronze Age (Andrades Valtueña et al., 2017).

To investigate the presence of pathogen DNA signatures among individuals from the Lake Baikal region, we screened all analyzed specimens (n = 19) using the pipeline HOPS (Hübler et al., 2019). Our metagenomic analysis of shotgun sequenced data revealed evidence of ancient *Y. pestis* DNA in two Early Bronze Age individuals (GLZ001 and GLZ002) (Figure S5), which were dated to 4,556 and 4,430 BP (median dates), respectively, after accounting for the freshwater reservoir effect present in this region (Table S1). Subsequent whole-*Y. pestis*-genome enrichment yielded a 7.2-and 12.8-fold genomic coverage for GLZ001 and GLZ002, respectively (Table S6). We built a maximum likelihood phylogeny in order to compare the newly reconstructed genomes with previously published ancient and modern *Y. pestis* isolates (Figure 4B). GLZ001 and GLZ002 grouped on the previously described LNBA *Y. pestis* lineage (Andrades Valtueña et al., 2017; Rasmussen et al., 2015b), together with 4,800-to-3,500-year-old isolates from across Eurasia (Figure 4B). Specifically, they appeared most closely related (distance *d* = 17–19 SNPs) to a genome from the Baltic Sea region (Kunila2, 4,520–4,290 BP), retrieved from an individual culturally affiliated with the Corded Ware complex (Figure 4B; Andrades Valtueña et al., 2017). Such a result is intriguing since, based on human genetic analyses, individuals GLZ001 and GLZ002 appear as genetic outliers compared to other analyzed Bronze Age individuals from the same region. In addition, they lack Yamnaya-related Steppe ancestry (Figure 1; Figure 4A), common to all published plague victims with *Y. pestis* genomes grouping on the LNBA phylogenetic lineage (Andrades Valtueña et al., 2017; Rasmussen et al., 2015b).

To further characterize the *Y. pestis* genomic contents of GLZ001 and GLZ002, we computed the coverage across previously defined virulence-associated and evolutionary-determinant genes (Demeure et al., 2019; Zhou and Yang, 2009). Our

analysis revealed similar patterns to those previously observed in LNBA strains, which are consistent with a decreased efficiency in flea-mediated-transmission (Figure S5). These include the absence of *ymt* on the pMT1 plasmid and the presence of active PDE-2, PDE-3, *rcsA*, and *ureD* gene variants (Figures S5 and S6; Andrades Valtueña et al., 2017; Rasmussen et al., 2015b; Sun et al., 2014). Additionally, we identified here the absence of *ympt1.66c* (Figure S5), a putative helicase considered to be involved in the bacterium's initial within-macrophage survival and subsequent bubonic disease progression (Pradel et al., 2014).

Moreover, to investigate whether the radiocarbon date correction using stable isotope values could provide a reliable estimation of the freshwater reservoir offsets in GLZ001 and GLZ002, we explored an additional dating approach for these specimens based on the *Y. pestis* molecular phylogeny. For this, we first assessed the temporal phylogenetic signal across the LNBA lineage using previously published radiocarbon dates as tip calibrations (Andrades Valtueña et al., 2017; Rasmussen et al., 2015b). The resulting correlation coefficient (*r*) and R^2 values were 0.88 and 0.78, respectively (Figure S5), which supported a linear relationship between root-to-tip genetic distance and specimen age for this dataset (including a modern 0.PE2 genome as outgroup). As such, we used the Bayesian framework BEAST (Drummond and Rambaut, 2007) to independently re-estimate the tip dates of GLZ001 and GLZ002 and tested the coalescent constant size and coalescent skyline tree priors in combination with strict and lognormal relaxed clock models (see STAR Methods). All runs produced overlapping estimates supporting median ages of ~4,400 BP for both genomes (95% highest posterior density [HPD] range across all models: 4,115–4,590 BP) (Figure 4C; Table S6). As such, our analysis supports the estimated offset in the radiocarbon date estimates of both Glazkovskoe predmestie individuals, caused by the freshwater reservoir effect described previously for the Lake Baikal region (Schulting et al., 2014; Weber et al., 2016).

Taken together, these results provide evidence for the presence of human *Y. pestis* infections in the Lake Baikal region during the Early Bronze Age (Figure 4B). To our knowledge, this is the easternmost appearance of *Y. pestis* strains associated with the LNBA lineage, despite the lack of Steppe-related ancestry in both affected individuals.

Genetic Influence on the Okunevo Culture

The Okunevo is a Bronze Age culture of the central steppe, geographically located west of the Lake Baikal region (Figure 1A). Previous studies have suggested a genetic relationship between Okunevo and ancient Lake Baikal individuals (Damgaard et al., 2018b; Jeong et al., 2019). In this study, we detected a high genetic affinity between the Early Bronze Age BZK002 genome from the region where the Okunevo culture was subsequently practiced and Okunevo-related individuals (Damgaard et al., 2018a), as revealed by PCA and outgroup f_3 statistics (Figure 1C; Table S4). The BZK002 genome could be modeled with qpAdm as a two-way admixture between LNBA Baikal and AG3 or Botai-like populations, which are central Eurasian populations without any Steppe ancestry (Figure 5A). BZK002 also performed as a good proxy for the populations that mixed with Yamnaya/
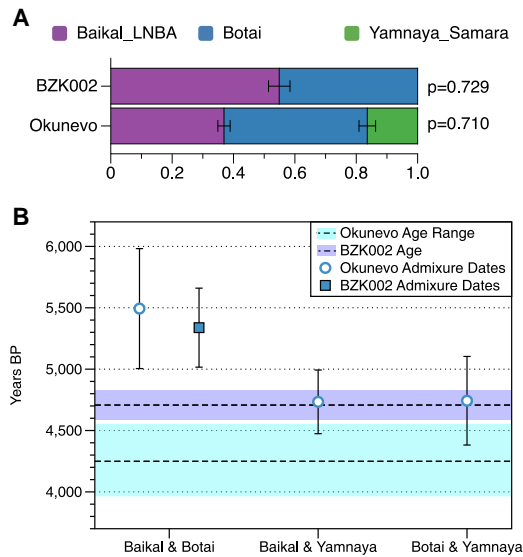
Figure 5. Genetic Relationship between BZK002 and Okunevo Population

(A) *qpAdm* modeling of BZK002 as 2-way admixture between LNBA Baikal and Botai populations and Okunevo as 3-way admixture of LNBA Baikal, Botai, and Yamnaya. The error bars show the standard errors of estimated ancestry proportions. Details of the modeling are provided in Table S3.

(B) Estimated admixture dates of LNBA Baikal, Botai, and Yamnaya ancestries in the Okunevo-related population and BZK002. The dashed lines show the median calibrated age of BZK002 and the average age of published Okunevo-related individuals. The shades show the 2-sigma range of BZK002 calibrated radiocarbon age and the range of Okunevo-related individual ages, respectively. The error bars of the estimated admixture dates show the cumulative range considering both standard errors of the admixture dating analysis and radiocarbon age ranges.

See also Figure S4 and Table S3.

Afanasievo-related groups to form the ancestry observed in Okunevo-associated individuals (Table S3). Moreover, we verified the modeling of Okunevo as a three-way admixture among the LNBA Baikal group, AG3 or Botai-like individuals, and Steppe-related populations (Figure 5A; Table S3).

Finally, we used *DATES* to estimate the timing of admixture events among those three ancestries in the Okunevo-related population, as well as to estimate the admixture timing of LNBA Baikal and Botai ancestries in the BZK002 individual. The estimated dates of these admixture events fell into two distinct time periods. Using LNBA Baikal and Botai-like populations as sources, the admixture events in Okunevo and BZK002 were dated to 42.9 and 23.4 generations ago, respectively, corresponding to an overlapping range of 6,000–5,000 BP, considering the specimens ages. The estimations including Yamnaya-related populations as one of the sources in Okunevo were instead both younger, around 17 generations, corresponding to 5,000–4,500 BP (Figure 5B; Figure S4; Table S5). Based on the dating results, we propose a scenario where the formation of the Okunevo-related gene pool resulted from an initial admixture of Botai-like and LNBA Baikal ancestries, followed by a gene flow of Yamnaya-related ancestry via its eastward expansion during the fifth millennium BP. BZK002 was directly radiocarbon

dated to around 4,700 BP, predating the published Okunevo-related individuals by 200–800 years and overlapping with the estimated time range of the Steppe-ancestry admixture. Moreover, the Baikal-Botai admixture for BZK002 falls within the same period estimated for the Okunevo population, suggesting that this individual could represent an intermediate status during the formation of the Okunevo-associated genetic profile.

DISCUSSION

In this study, we demonstrated that multiple population turnovers took place in the Lake Baikal region from the Upper Paleolithic to the Bronze Age periods as a dynamic variation of ANE and NEA ancestry proportions. However, instead of the suggested complete replacement of the ANE-related ancestry by an East Asian gene pool (Damgaard et al., 2018a), we show that the ancestry first described in the 24,000-year-old MA1 individual survived in the region throughout the Upper Paleolithic until the Bronze Age, as revealed in the genome of the 14,000-year-old UKY individual as well as in the Early Neolithic population. Furthermore, the genetic transition from Early Neolithic to Bronze Age Baikal groups could be well explained by a prolonged gene flow between NEA- and ANE-related ancestries throughout the eighth to the sixth millennium BP (Figure 3B), and the UKY genome was attested to be a better local source for the ANE ancestry than a possible southward expansion of Kolyma-related ancestry (Sikora et al., 2019). In contrast, the Kolyma genome represents a good proxy for the Paleo-Eskimo Saqqaq genetic profile, supporting the view that the Paleo-Eskimo ancestry emerged around northeastern Siberia (Flegontov et al., 2019), though we are unable to rule out the scenario that this ancestry formed in central or southern Siberia from an UKY-related gene pool.

Noticeably, we detect a strong genetic connection between Upper Paleolithic Siberians from the Lake Baikal region with non-Arctic Native Americans. According to our demographic modeling, Native Americans, the 14,000-year-old southern Siberian UKY individual and the 9,800-year-old northeastern Siberian Kolyma individual were all descendants, at least in part, of the same admixed population that carried both ANE and NEA ancestries. This population was likely widespread across Siberia during the Upper Paleolithic and experienced frequent genetic contacts with northeast Asian-related populations, which resulted in varying proportions of ANE/NEA ancestry through different areas and time periods. Considering the earlier population split of UKY compared with Kolyma and the Alaskan USR1 genome from the lineage leading to the rest of Native American populations, our result challenges the hypothesis that this basal Native American ancestry formed in northeastern Siberia (Sikora et al., 2019). Further genetic evidence from Upper Paleolithic Siberian groups will be necessary to describe where and when exactly the ancestral gene pool of Native Americans came together.

Moreover, we provided evidence for the genetic contact between southern Siberia and the western steppe during the Early Bronze Age, based on both human and pathogen DNA data, which suggests a high mobility across Eurasia. The genetic influence of Yamnaya-related populations in the Lake Baikal region is evident by the presence of Steppe ancestry in individual KPT005 (Figure 4A). In addition, previous studies have

suggested that such migrations likely also facilitated the spread of the *Y. pestis* LNBA lineage across Eurasia (Andrades Valtueña et al., 2017), as all individuals associated with this lineage carry Steppe ancestry (Allentoft et al., 2015; Andrades Valtueña et al., 2017; Haak et al., 2015; Mathieson et al., 2018; Mittnik et al., 2018, 2019; Wang et al., 2019). In this study, the two individuals shown to be infected with *Yersinia pestis* (GLZ001 and GLZ002) did not display genetic evidence of Yamnaya-related Steppe ancestry in their genomes but had substantially more NEA ancestry than all other Bronze Age individuals from the same and other surrounding sites (Figure 1). Moreover, one of the two individuals (GLZ001) showed a non-local signal in strontium isotope analysis, supporting a homeland outside the Angara River Valley. Instead, based on the *Y. pestis* phylogeny, the newly reconstructed Baikal genomes were found to be genetically closest related to a strain from the Baltic region in northeastern Europe (Figure 4B), isolated from an individual associated with the Corded Ware complex (Andrades Valtueña et al., 2017; Mittnik et al., 2018). Although our current resolution is insufficient for inferring patterns of pathogen transmission between western Eurasia and southern Siberia, the presented data may rather be indicative of a century- or decade-long process that lead to the bacterium's long-distance spread. Nevertheless, the phylogenetic topology of both Lake Baikal genomes within the LNBA lineage most parsimoniously suggests that *Y. pestis* spread into this region within the context of Yamnaya-related steppe expansions during the fifth millennium BP (Andrades Valtueña et al., 2017). Importantly, our results provide prime evidence that strains of the LNBA *Y. pestis* lineage also affected individuals that were not genetically impacted by such migrations.

In conclusion, our study describes dynamic changes in the population structure of the Lake Baikal region and reveals a widespread occurrence of the genetic ancestry that gave rise to the First People of the Americas in Upper Paleolithic Siberia. In addition, we provide evidence of high human mobility across the Eurasian steppe revealing new insights about the spread of *Y. pestis* during the fifth millennium BP.

STAR★METHODS

Detailed methods are provided in the online version of this paper and include the following:

- KEY RESOURCES TABLE
- RESOURCE AVAILABILITY
  - Lead Contact
  - Materials Availability
  - Data and Code Availability
- EXPERIMENTAL MODEL AND SUBJECT DETAILS
  - Archaeological information
- METHOD DETAILS
  - Radiocarbon dating and calibration
  - Stable isotope analysis
  - Strontium isotope analysis
  - Ancient DNA processing
  - Human genome enrichment and sequencing
  - *Y. pestis* genome enrichment

- QUANTIFICATION AND STATISTICAL ANALYSIS
  - Genotyping and dataset preparation for analysis
  - Population genetics analysis
  - Admixture modeling with *qpAdm*
  - Demographic modeling with *qpGraph*
  - Admixture dating with *DATES*
  - Pathogen DNA screening with HOPS
  - Read processing, SNP calling and phylogenetic analysis of *Yersinia pestis*
  - BEAST v1.8 tip dating of GLZ001 and GLZ002
  - Assessment of *Y. pestis* gene profiles

REFERENCES

Alekseev, V.P., and Mamonova, N.N. (1979). K paleoantropologii epohi neolita verhov'ev Leny. Sov. Etnogr. *5*, 49–63.

Alexander, D.H., Novembre, J., and Lange, K. (2009). Fast model-based estimation of ancestry in unrelated individuals. Genome Res. *19*, 1655–1664.

Alexander Bentley, R. (2006). Strontium Isotopes from the Earth to the Archaeological Skeleton: A Review. J. Archaeol. Method Theory *13*, 135–187.

Allentoft, M.E., Sikora, M., Sjögren, K.-G., Rasmussen, S., Rasmussen, M., Stenderup, J., Damgaard, P.B., Schroeder, H., Ahlström, T., Vinner, L., et al. (2015). Population genomics of Bronze Age Eurasia. Nature *522*, 167–172.

Ambrose, S.H., and Norr, L. (1993). Experimental Evidence for the Relationship of the Carbon Isotope Ratios of Whole Diet and Dietary Protein to Those of Bone Collagen and Carbonate. In Prehistoric Human Bone: Archaeology at the Molecular Level, J.B. Lambert and G. Grupe, eds. (Springer Berlin Heidelberg), pp. 1–37.

Andrades Valtueña, A., Mittnik, A., Key, F.M., Haak, W., Allmäe, R., Belinskij, A., Daubaras, M., Feldman, M., Jankauskas, R., Janković, I., et al. (2017).

Cell
Article

CellPress

The Stone Age Plague and Its Persistence in Eurasia. Curr. Biol. *27*, 3683–3691.

Auton, A., Brooks, L.D., Durbin, R.M., Garrison, E.P., Kang, H.M., Korbel, J.O., Marchini, J.L., McCarthy, S., McVean, G.A., and Abecasis, G.R.; 1000 Genomes Project Consortium (2015). A global reference for human genetic variation. Nature *526*, 68–74.

Bazalijskij, V.I. (2012). Pogrebal'nye kompleksy epohi pozdnego mezolita – neolita Bajkal'skoj Sibiri: tradicii pogrebenij, absoljutnyj vozrast. Izv. Lab. Drevnih Tekhnologij. Irkutsk Izd-vo IrGTU. *9*, 43–101.

Bentley, R.A., Krause, R., Price, T.D., and Kaufmann, B. (2003). Human mobility at the early neolithic settlement of vaihingen, germany: evidence from strontium isotope analysis*. Archaeometry *45*, 471–486.

Bentley, R.A., Price, T.D., and Stephan, E. (2004). Determining the 'local' 87Sr/86Sr range for archaeological skeletons: a case study from Neolithic Europe. J. Archaeol. Sci. *31*, 365–375.

Bos, K.I., Schuenemann, V.J., Golding, G.B., Burbano, H.A., Waglechner, N., Coombes, B.K., McPhee, J.B., DeWitte, S.N., Meyer, M., Schmedes, S., et al. (2011). A draft genome of Yersinia pestis from victims of the Black Death. Nature *478*, 506–510.

Bos, K.I., Herbig, A., Sahl, J., Waglechner, N., Fourment, M., Forrest, S.A., Klunk, J., Schuenemann, V.J., Poinar, D., Kuch, M., et al. (2016). Eighteenth century Yersinia pestis genomes reveal the long-term persistence of an historical plague focus. eLife *5*, e12994.

Briggs, A.W., Stenzel, U., Meyer, M., Krause, J., Kircher, M., and Pääbo, S. (2010). Removal of deaminated cytosines and detection of in vivo methylation in ancient DNA. Nucleic Acids Res. *38*, e87.

Brock, F., Higham, T., and Ramsey, C.B. (2013). Comments on the Use of Ezee-Filters™ and Ultrafilters at Orau. Radiocarbon *55*, 211–212.

Browning, B.L., and Browning, S.R. (2013). Improving the accuracy and efficiency of identity-by-descent detection in population data. Genetics *194*, 459–471.

Capo, R.C., Stewart, B.W., and Chadwick, O.A. (1998). Strontium isotopes as tracers of ecosystem processes: theory and methods. Geoderma *82*, 197–225.

Cui, Y., Yu, C., Yan, Y., Li, D., Li, Y., Jombart, T., Weinert, L.A., Wang, Z., Guo, Z., Xu, L., et al. (2013). Historical variations in mutation rate in an epidemic pathogen, Yersinia pestis. Proc. Natl. Acad. Sci. USA *110*, 577–582.

Dabney, J., Knapp, M., Glocke, I., Gansauge, M.-T., Weihmann, A., Nickel, B., Valdiosera, C., García, N., Pääbo, S., Arsuaga, J.-L., and Meyer, M. (2013). Complete mitochondrial genome sequence of a Middle Pleistocene cave bear reconstructed from ultrashort DNA fragments. Proc. Natl. Acad. Sci. USA *110*, 15758–15763.

Damgaard, P. de B., Martiniano, R., Kamm, J., Moreno-Mayar, J.V., Kroonen, G., Peyrot, M., Barjamovic, G., Rasmussen, S., Zacho, C., Baimukhanov, N., et al. (2018a). The first horse herders and the impact of early Bronze Age steppe expansions into Asia. Science *360*, eaar7711.

Damgaard, P.B., Marchi, N., Rasmussen, S., Peyrot, M., Renaud, G., Korneliussen, T., Moreno-Mayar, J.V., Pedersen, M.W., Goldberg, A., Usmanova, E., et al. (2018b). 137 ancient human genomes from across the Eurasian steppes. Nature *557*, 369–374.

Debets, G.F. (1930). Antropologicheskij sostav drevnego naseleniya Pribajkal'ya v epohu pozdnego neolita. Rus. Antropol. Zhurnal *t. XIX*, 1–2, 7–50.

Debets, G.F. (1948). Paleoantropologiya SSSR / TIE, novaya seriya (M.-L. T. IV.).

Delaneau, O., Zagury, J.-F., and Marchini, J. (2013). Improved whole-chromosome phasing for disease and population genetic studies. Nat. Methods *10*, 5–6.

Demeure, C.E., Dussurget, O., Mas Fiol, G., Le Guern, A.-S., Savin, C., and Pizarro-Cerdá, J. (2019). Yersinia pestis and plague: an updated view on evolution, virulence determinants, immune subversion, vaccination, and diagnostics. Genes Immun. *20*, 357–370.

Deniro, M.J., and Epstein, S. (1981). Influence of diet on the distribution of nitrogen isotopes in animals. Geochim. Cosmochim. Acta *45*, 341–351.

DePristo, M.A., Banks, E., Poplin, R., Garimella, K.V., Maguire, J.R., Hartl, C., Philippakis, A.A., del Angel, G., Rivas, M.A., Hanna, M., et al. (2011). A framework for variation discovery and genotyping using next-generation DNA sequencing data. Nat. Genet. *43*, 491–498.

Drummond, A.J., and Rambaut, A. (2007). BEAST: Bayesian evolutionary analysis by sampling trees. BMC Evol. Biol. *7*, 214.

Eroshenko, G.A., Nosov, N.Y., Krasnov, Y.M., Oglodin, Y.G., Kukleva, L.M., Guseva, N.P., Kuznetsov, A.A., Abdikarimov, S.T., Dzhaparova, A.K., and Kutyrev, V.V. (2017). Yersinia pestis strains of ancient phylogenetic branch 0.ANT are widely spread in the high-mountain plague foci of Kyrgyzstan. PLoS ONE *12*, e0187230.

Feldman, M., Harbeck, M., Keller, M., Spyrou, M.A., Rott, A., Trautmann, B., Scholz, H.C., Päffgen, B., Peters, J., McCormick, M., et al. (2016). A High-Coverage Yersinia pestis Genome from a Sixth-Century Justinianic Plague Victim. Mol. Biol. Evol. *33*, 2911–2923.

Flegontov, P., Altınışık, N.E., Changmai, P., Rohland, N., Mallick, S., Adamski, N., Bolnick, D.A., Broomandkhoshbacht, N., Candilio, F., Culleton, B.J., et al. (2019). Palaeo-Eskimo genetic ancestry and the peopling of Chukotka and North America. Nature *570*, 236–240.

Fu, Q., Meyer, M., Gao, X., Stenzel, U., Burbano, H.A., Kelso, J., and Pääbo, S. (2013). DNA analysis of an early modern human from Tianyuan Cave, China. Proc. Natl. Acad. Sci. USA *110*, 2223–2227.

Fu, Q., Hajdinjak, M., Moldovan, O.T., Constantin, S., Mallick, S., Skoglund, P., Patterson, N., Rohland, N., Lazaridis, I., Nickel, B., et al. (2015). An early modern human from Romania with a recent Neanderthal ancestor. Nature *524*, 216–219.

Fu, Q., Posth, C., Hajdinjak, M., Petr, M., Mallick, S., Fernandes, D., Furtwängler, A., Haak, W., Meyer, M., Mittnik, A., et al. (2016). The genetic history of Ice Age Europe. Nature *534*, 200–205.

Fuller, B.T., Richards, M.P., and Mays, S.A. (2003). Stable carbon and nitrogen isotope variations in tooth dentine serial sections from Wharram Percy. J. Archaeol. Sci. *30*, 1673–1684.

Gansauge, M.-T., Gerber, T., Glocke, I., Korlević, P., Lippik, L., Nagel, S., Riehl, L.M., Schmidt, A., and Meyer, M. (2017). Single-stranded DNA library preparation from highly degraded DNA using T4 DNA ligase. Nucleic Acids Res. *45*, e79–e79.

Garcia, E., Chain, P., Worsham, P., Bearden, S.W., Malfatti, S., Lang, D., Larimer, F., and Lindler, L. (2007). Pestoides F, an Atypical Yersinia pestis Strain from the Former Soviet Union. Adv. Exp. Med. Biol. *603*, 17–22.

Graustein, W.C., and Armstrong, R.L. (1983). The use of strontium-87/strontium-86 ratios to measure atmospheric transport into forested watersheds. Science *219*, 289–292.

Haak, W., Lazaridis, I., Patterson, N., Rohland, N., Mallick, S., Llamas, B., Brandt, G., Nordenfelt, S., Harney, E., Stewardson, K., et al. (2015). Massive migration from the steppe was a source for Indo-European languages in Europe. Nature *522*, 207–211.

Haverkort, C.M., Bazaliiskii, V.I., and Savel'ev, N.A. (2010). Identifying hunter-gatherer mobility patterns using strontium isotopes. In Prehistoric Hunter-Gatherers of the Baikal Region, Siberia, A. Weber, A. Katzenberg, and T.G. Schurr, eds. (Penn Press), pp. 217–238.

Hillson, S. (1996). Dental Anthropology (Cambridge University Press).

Hübler, R., Key, F.M., Warinner, C., Bos, K.I., Krause, J., and Herbig, A. (2019). HOPS: automated detection and authentication of pathogen DNA in archaeological remains. Genome Biol. *20*, 280.

Jeong, C., Wilkin, S., Amgalantugs, T., Bouwman, A.S., Taylor, W.T.T., Hagan, R.W., Bromage, S., Tsolmon, S., Trachsel, C., Grossmann, J., et al. (2018). Bronze Age population dynamics and the rise of dairy pastoralism on the eastern Eurasian steppe. Proc. Natl. Acad. Sci. USA *115*, E11248–E11255.

Jeong, C., Balanovsky, O., Lukianova, E., Kahbatkyzy, N., Flegontov, P., Zaporozhchenko, V., Immel, A., Wang, C.C., Ixan, O., Khussainova, E., et al. (2019). The genetic history of admixture across inner Eurasia. Nat. Ecol. Evol. *3*, 966–976.

Jones, E.R., Gonzalez-Fortes, G., Connell, S., Siska, V., Eriksson, A., Martiniano, R., McLaughlin, R.L., Gallego Llorente, M., Cassidy, L.M., Gamba, C., et al. (2015). Upper Palaeolithic genomes reveal deep roots of modern Eurasians. Nat. Commun. 6, 8912.

Jónsson, H., Ginolhac, A., Schubert, M., Johnson, P.L.F., and Orlando, L. (2013). mapDamage2.0: fast approximate Bayesian estimates of ancient DNA damage parameters. Bioinformatics 29, 1682–1684.

Jørkov, M.L.S., Heinemeier, J., and Lynnerup, N. (2009). The petrous bone–a new sampling site for identifying early dietary patterns in stable isotopic studies. Am. J. Phys. Anthropol. 138, 199–209.

Katzenberg, M.A., and Weber, A. (1999). Stable isotope ecology and palaeodiet in the Lake Baikal region of Siberia. J. Archaeol. Sci. 26, 651–659.

Katzenberg, M.A., Bazaliiskii, V.I., Goriunova, O.I., Savel'ev, N.A., and Weber, A.W. (2010). 8. Diet Reconstruction of Prehistoric Hunter-Gatherers in the Lake Baikal Region. In Prehistoric Hunter-Gatherers of the Baikal Region, Siberia, A.W. Weber, M.A. Katzenberg, and T.G. Schurr, eds. (University of Pennsylvania Press), pp. 175–192.

Keller, M., Spyrou, M.A., Scheib, C.L., Neumann, G.U., Kröpelin, A., Haas-Gebhard, B., Päffgen, B., Haberstroh, J., Ribera I Lacomba, A., Raynaud, C., et al. (2019). Ancient Yersinia pestis genomes from across Western Europe reveal early diversification during the First Pandemic (541–750). Proc. Natl. Acad. Sci. USA 116, 12363–12372.

Kircher, M., Sawyer, S., and Meyer, M. (2012). Double indexing overcomes inaccuracies in multiplex sequencing on the Illumina platform. Nucleic Acids Res. 40, e3.

Kislichkina, A.A., Bogun, A.G., Kadnikova, L.A., Maiskaya, N.V., Platonov, M.E., Anisimov, N.V., Galkina, E.V., Dentovskaya, S.V., and Anisimov, A.P. (2015). Nineteen Whole-Genome Assemblies of Yersinia pestis subsp. microtus, Including Representatives of Biovars caucasica, talassica, hissarica, altaica, xilingolensis, and ulegeica. Genome Announc. 3, e01342-15.

Kislichkina, A.A., Bogun, A.G., Kadnikova, L.A., Maiskaya, N.V., Solomentsev, V.I., Dentovskaya, S.V., Balakhonov, S.V., and Anisimov, A.P. (2018a). Nine Whole-Genome Assemblies of Yersinia pestis subsp. microtus bv. Altaica Strains Isolated from the Altai Mountain Natural Plague Focus (No. 36) in Russia. Genome Announc. 6, e01440-17.

Kislichkina, A.A., Bogun, A.G., Kadnikova, L.A., Maiskaya, N.V., Solomentsev, V.I., Sizova, A.A., Dentovskaya, S.V., Balakhonov, S.V., and Anisimov, A.P. (2018b). Six Whole-Genome Assemblies of Yersinia pestis subsp. microtus bv. ulegeica (Phylogroup 0.PE5) Strains Isolated from Mongolian Natural Plague Foci. Genome Announc. 6, e00536-18.

Kiyashko, S.I., Richard, P., Chandler, T., Kozlova, T.A., and Williams, D.F. (1998). Stable carbon isotope ratios differentiate autotrophs supporting animal diversity in Lake Baikal. Comptes Rendus l'Académie Des Sci. - Ser. III - Sci. Vine 321, 509–516.

Korlević, P., Gerber, T., Gansauge, M.-T., Hajdinjak, M., Nagel, S., Aximu-Petri, A., and Meyer, M. (2015). Reducing microbial and human contamination in DNA extractions from ancient bones and teeth. Biotechniques 59, 87–93.

Korneliussen, T.S., Albrechtsen, A., and Nielsen, R. (2014). ANGSD: Analysis of Next Generation Sequencing Data. BMC Bioinformatics 15, 356.

Kutyrev, V.V., Eroshenko, G.A., Motin, V.L., Nosov, N.Y., Krasnov, J.M., Kukleva, L.M., Nikiforov, K.A., Al'khova, Z.V., Oglodin, E.G., and Guseva, N.P. (2018). Phylogeny and Classification of Yersinia pestis Through the Lens of Strains From the Plague Foci of Commonwealth of Independent States. Front. Microbiol. 9, 1106.

Lazaridis, I., Patterson, N., Mittnik, A., Renaud, G., Mallick, S., Kirsanow, K., Sudmant, P.H., Schraiber, J.G., Castellano, S., Lipson, M., et al. (2014). Ancient human genomes suggest three ancestral populations for present-day Europeans. Nature 513, 409–413.

Lazaridis, I., Nadel, D., Rollefson, G., Merrett, D.C., Rohland, N., Mallick, S., Fernandes, D., Novak, M., Gamarra, B., Sirak, K., et al. (2016). Genomic insights into the origin of farming in the ancient Near East. Nature 536, 419–424.

Li, H., and Durbin, R. (2009). Fast and accurate short read alignment with Burrows-Wheeler transform. Bioinformatics 25, 1754–1760.

Li, H., Handsaker, B., Wysoker, A., Fennell, T., Ruan, J., Homer, N., Marth, G., Abecasis, G., and Durbin, R.; 1000 Genome Project Data Processing Subgroup (2009). The sequence alignment/map format and SAMtools. Bioinformatics 25, 2078–2079.

Longin, R. (1971). New method of collagen extraction for radiocarbon dating. Nature 230, 241–242.

Mamonova, N.N. (1973). K voprosu o drevnem naselenii Priangar'ya po paleoantropologicheskim dannym. In Problemy Arheologii Urala i Sibiri, A.P. Smirnov, ed. (M. Nauka), pp. 8–29.

Mamonova, N.N., and Sulerzhickij, L.D. (1989). Radiouglerodnaya khronologiya golocenovyh pogrebenij Pribajkal'ya i Zabajkal'ya po osteologicheskomu materialu iz mogil'nikov. Sov. Arkheologiya 1, 19–32.

Mamonova, N.N., and Sulerzhickij, L.D. (2008). Radiouglerodnaya khronologiya golocenovyh pogrebenij Pribajkal'ya i Zabajkal'ya po osteologicheskomu materialu iz mogil'nikov. In Chelovek, Adaptaciya, Kul'tura (M. IA RAN), pp. 127–138.

Mathieson, I., Lazaridis, I., Rohland, N., Mallick, S., Patterson, N., Roodenberg, S.A., Harney, E., Stewardson, K., Fernandes, D., Novak, M., et al. (2015). Genome-wide patterns of selection in 230 ancient Eurasians. Nature 528, 499–503.

Mathieson, I., Alpaslan-Roodenberg, S., Posth, C., Szécsényi-Nagy, A., Rohland, N., Mallick, S., Olalde, I., Broomandkhoshbacht, N., Candilio, F., Cheronet, O., et al. (2018). The genomic history of southeastern Europe. Nature 555, 197–203.

Meyer, M., and Kircher, M. (2010). Illumina Sequencing Library Preparation for Highly Multiplexed Target Capture and Sequencing. Cold Spring Harb. Protoc. 2010, pdb.prot5448-pdb.prot5448.

Minagawa, M., and Wada, E. (1984). Stepwise enrichment of 15N along food chains: Further evidence and the relation between δ15N and animal age. Geochim. Cosmochim. Acta 48, 1135–1140.

Minnich, S.A., and Rohde, H.N. (2007). A rationale for repression and/or loss of motility by pathogenic yersinia in the mammalian host. In The Genus Yersinia: From Genomics to Function, R.D. Perry and J.D. Fetherston, eds. (Springer), pp. 298–311.

Mittnik, A., Wang, C.C., Pfrengle, S., Daubaras, M., Zariņa, G., Hallgren, F., Allmäe, R., Khartanovich, V., Moiseyev, V., Tõrv, M., et al. (2018). The genetic prehistory of the Baltic Sea region. Nat. Commun. 9, 1–11.

Mittnik, A., Massy, K., Knipper, C., Wittenborn, F., Friedrich, R., Pfrengle, S., Burri, M., Carlichi-Witjes, N., Deeg, H., Furtwängler, A., et al. (2019). Kinship-based social inequality in Bronze Age Europe. Science 366, 731–734.

Montgomery, J. (2010). Passports from the past: Investigating human dispersals using strontium isotope analysis of tooth enamel. Ann. Hum. Biol. 37, 325–346.

Moorjani, P., and Patterson, N.. https://github.com/priyamoorjani/DATES.

Morelli, G., Song, Y., Mazzoni, C.J., Eppinger, M., Roumagnac, P., Wagner, D.M., Feldkamp, M., Kusecek, B., Vogler, A.J., Li, Y., et al. (2010). Yersinia pestis genome sequencing identifies patterns of global phylogenetic diversity. Nat. Genet. 42, 1140–1143.

Moreno-Mayar, J.V., Potter, B.A., Vinner, L., Steinrücken, M., Rasmussen, S., Terhorst, J., Kamm, J.A., Albrechtsen, A., Malaspinas, A.S., Sikora, M., et al. (2018). Terminal Pleistocene Alaskan genome reveals first founding population of Native Americans. Nature 553, 203–207.

Movsesian, A.A., Bakholdina, V.Y., and Pezhemsky, D.V. (2014). Biological diversity and population history of Middle Holocene hunter-gatherers from the Cis-Baikal region of Siberia. Am. J. Phys. Anthropol. 155, 559–570.

Movsesian, A.A., Bakholdina, V.Y., and Pezhemsky, D.V. (2015). Sushchestvovala li geneticheskaya preemstvennost' mezhdu naseleniem razlichnyh etapov Pribajkal'skogo neolita? Vestn. Mosk. Univ. Seriya 23 Antropol. 3, 94–104.

Namouchi, A., Guellil, M., Kersten, O., Hänsch, S., Ottoni, C., Schmid, B.V., Pacciani, E., Quaglia, L., Vermunt, M., Bauer, E.L., et al. (2018). Integrative approach using Yersinia pestis genomes to revisit the historical landscape of plague during the Medieval Period. Proc. Natl. Acad. Sci. USA 115, E11790–E11797.

Nier, A.O. (1938). The Isotopic Constitution of Strontium, Barium, Bismuth, Thallium and Mercury. Phys. Rev. *54*, 275–278.

Nomokonova, T., Losey, R.J., Goriunova, O.I., and Weber, A.W. (2013). A freshwater old carbon offset in Lake Baikal, Siberia and problems with the radiocarbon dating of archaeological sediments: Evidence from the Sagan-Zaba II site. Quat. Int. *290–291*, 110–125.

Okladnikov, A.P. (1926). Neoliticheskie stoyanki na Verhnej Lene. Kraeved. v Irkutsk. Gubernii Zap.Stud. Nauch. Kruzhka Kraeved. Pri Irkut. Gos. Un-Te *3*, 29–38.

Okladnikov, A.P. (1928). Neoliticheskij mogil'nik v mestnosti Hapcagaj (Verhnyaya Lena). Izv. VSORGO *53*, 125–134.

Okladnikov, A.P. (1929). Raskopki v Kachugskom rajone po pritokam Leny. Vlast' Tr. *10*, Avg *185*, 4.

Okladnikov, A.P. (1950). Neolit i bronzovyj vek Pribajkal'ya. Istoriko-arheologicheskoe issledovanie. CH. I, II. Mater. i Issled. Po Arheol. SSSR *18*, M.-L. 412s.

Okladnikov, A.P. (1955). Neolit i bronzovyj vek Pribajkal'ya. CH. III. (Glazkovskoe vremya). Mater. i Issled. Po Arheol. SSSR *43*, M.-L. 373 s.

Okladnikov, A.P. (1977). Otchet ob issledovanii paleoliticheskogo poseleniia Ust'-Kyakhta v 1976 g. In Archive of the Institut Arkheologii i Etnografii Sibirskogo Otdeleniia Rossiiskoi Akademii Nauk (Novosibirsk), p. 78.

Okladnikov, A.P. (1979). Nauchnyi otchet o raskopkakh stoianki Ust'-Kyakhta 1 (Kyakhtinskii raion BurASSR) v 1978 g. In Archive of the Institut Arkheologii i Etnografii Sibirskogo Otdeleniia Rossiiskoi Akademii Nauk (Novosibirsk), p. 21.

Olalde, I., Brace, S., Allentoft, M.E., Armit, I., Kristiansen, K., Booth, T., Rohland, N., Mallick, S., Szécsényi-Nagy, A., Mittnik, A., et al. (2018). The Beaker phenomenon and the genomic transformation of northwest Europe. Nature *555*, 190–196.

Orlova, L.A. (1995). Radiocarbon dating of archaeological sites of Siberia and the Far East. In Methods of Natural Sciences in Archaeological Reconstructions, A.P. Derevianko and Y.P. Kholushkin, eds. (Publishing House of the Institute of Archeology and Ethnography SB RAS), pp. 207–232.

Patterson, N., Price, A.L., and Reich, D. (2006). Population structure and eigenanalysis. PLoS Genet. *2*, e190.

Patterson, N., Moorjani, P., Luo, Y., Mallick, S., Rohland, N., Zhan, Y., Genschoreck, T., Webster, T., and Reich, D. (2012). Ancient admixture in human history. Genetics *192*, 1065–1093.

Pavlenok, G.D. (2014). Kostyanaya industriya stoyanki Ust'-Kyakhta-3 (Zapadnoe Zabajkal'e) [Bone industry of Ust'-Kyakhta Site (Western Trans-Baikalia)]. Gumanit. Nauk. v Sib. Humanities Sib. *2*, 14–18.

Pavlenok, G.D. (2015a). Tekhnologiya obrabotki kamnya v selenginskoi kulture Zapadnogo Zabaikaliya (po materialam stoyanki Ust-Kyakhta-3) (Altai State University).

Pavlenok, G.D. (2015b). Tekhnologiya izgotovleniya klinovidnyh nukleusov v selenginskoj kul'ture Zapadnogo Zabajkal'ya (po materialam stoyanki Ust-Kyakhta-3). Izv. Altaiskogo Gos. Univ. Istor. Nauk. i Arkheologiia [Bulletin Altai State Univ. Hist. Sci. Archaeol. *87*, 178–184.

Pavlenok, G.D., and Zubova, A.V. (2019). New Dental Finds Associated with the Paleolithic Selenga Culture, Western Trans-Baikal Region. Archaeol. Ethnol. Anthropol. Eurasia *47*, 3–11.

Peltzer, A., Jäger, G., Herbig, A., Seitz, A., Kniep, C., Krause, J., and Nieselt, K. (2016). EAGER: efficient ancient genome reconstruction. Genome Biol. *17*, 60.

Pin, C., Briot, D., Bassin, C., and Poitrasson, F. (1994). Concomitant separation of strontium and samarium-neodymium for isotopic analysis in silicate samples, based on specific extraction chromatography. Anal. Chim. Acta *298*, 209–217.

Posth, C., Nakatsuka, N., Lazaridis, I., Skoglund, P., Mallick, S., Lamnidis, T.C., Rohland, N., Nägele, K., Adamski, N., Bertolini, E., et al. (2018). Reconstructing the Deep Population History of Central and South America. Cell *175*, 1185–1197.

Poznik, G.D. (2016). Identifying Y-chromosome haplogroups in arbitrarily large samples of sequenced or genotyped men. bioRxiv. https://doi.org/10.1101/088716.

Pradel, E., Lemaître, N., Merchez, M., Ricard, I., Reboul, A., Dewitte, A., and Sebbane, F. (2014). New insights into how Yersinia pestis adapts to its mammalian host during bubonic plague. PLoS Pathog. *10*, e1004029.

Price, T.D., Swick, R.W., and Chase, E.P. (1986). Bone chemistry and prehistoric diet: strontium studies of laboratory rats. Am. J. Phys. Anthropol. *70*, 365–375.

Price, T.D., Burton, J.H., and Bentley, R.A. (2002). The Characterization of Biologically Available Strontium Isotope Ratios for the Study of Prehistoric Migration. Archaeometry *44*, 117–135.

Purcell, S., Neale, B., Todd-Brown, K., Thomas, L., Ferreira, M.A.R., Bender, D., Maller, J., Sklar, P., de Bakker, P.I.W., Daly, M.J., and Sham, P.C. (2007). PLINK: a tool set for whole-genome association and population-based linkage analyses. Am. J. Hum. Genet. *81*, 559–575.

Quinlan, A.R., and Hall, I.M. (2010). BEDTools: a flexible suite of utilities for comparing genomic features. Bioinformatics *26*, 841–842.

R Development Core Team (2008). Computational Many-Particle Physics (Springer Berlin Heidelberg).

Raghavan, M., Skoglund, P., Graf, K.E., Metspalu, M., Albrechtsen, A., Moltke, I., Rasmussen, S., Stafford, T.W., Jr., Orlando, L., Metspalu, E., et al. (2014a). Upper Palaeolithic Siberian genome reveals dual ancestry of Native Americans. Nature *505*, 87–91.

Raghavan, M., DeGiorgio, M., Albrechtsen, A., Moltke, I., Skoglund, P., Korneliussen, T.S., Grønnow, B., Appelt, M., Gulløv, H.C., Friesen, T.M., et al. (2014b). The genetic prehistory of the New World Arctic. Science *345*, 1255832–1255832.

Raghavan, M., Steinrücken, M., Harris, K., Schiffels, S., Rasmussen, S., DeGiorgio, M., Albrechtsen, A., Valdiosera, C., Ávila-Arcos, M.C., Malaspinas, A.-S., et al. (2015). Population genetics. Genomic evidence for the Pleistocene and recent population history of Native Americans. Science *349*, aab3884–aab3884.

Ramsey, C.B., Schulting, R., Goriunova, O.I., Bazaliiskii, V.I., and Weber, A.W. (2014). Analyzing Radiocarbon Reservoir Offsets Through Stable Nitrogen Isotopes and Bayesian Modeling: A Case Study Using Paired Human and Faunal Remains from the Cis-Baikal Region, Siberia. Radiocarbon *56*, 789–799.

Rascovan, N., Sjögren, K.-G., Kristiansen, K., Nielsen, R., Willerslev, E., Desnues, C., and Rasmussen, S. (2019). Emergence and Spread of Basal Lineages of Yersinia pestis during the Neolithic Decline. Cell *176*, 295–305.

Rasmussen, M., Li, Y., Lindgreen, S., Pedersen, J.S., Albrechtsen, A., Moltke, I., Metspalu, M., Metspalu, E., Kivisild, T., Gupta, R., et al. (2010). Ancient human genome sequence of an extinct Palaeo-Eskimo. Nature *463*, 757–762.

Rasmussen, M., Anzick, S.L., Waters, M.R., Skoglund, P., DeGiorgio, M., Stafford, T.W., Jr., Rasmussen, S., Moltke, I., Albrechtsen, A., Doyle, S.M., et al. (2014). The genome of a Late Pleistocene human from a Clovis burial site in western Montana. Nature *506*, 225–229.

Rasmussen, M., Sikora, M., Albrechtsen, A., Korneliussen, T.S., Moreno-Mayar, J.V., Poznik, G.D., Zollikofer, C.P.E., de León, M.P., Allentoft, M.E., Moltke, I., et al. (2015a). The ancestry and affiliations of Kennewick Man. Nature *523*, 455–458.

Rasmussen, S., Allentoft, M.E., Nielsen, K., Orlando, L., Sikora, M., Sjögren, K.-G., Pedersen, A.G., Schubert, M., Van Dam, A., Kapel, C.M.O., et al. (2015b). Early divergent strains of Yersinia pestis in Eurasia 5,000 years ago. Cell *163*, 571–582.

Reich, D., Thangaraj, K., Patterson, N., Price, A.L., and Singh, L. (2009). Reconstructing Indian population history. Nature *461*, 489–494.

Reimer, P.J., Bard, E., Bayliss, A., Beck, J.W., Blackwell, P.G., Ramsey, C.B., Buck, C.E., Cheng, H., Edwards, R.L., Friedrich, M., et al. (2013). IntCal13 and Marine13 Radiocarbon Age Calibration Curves 0–50,000 Years cal BP. Radiocarbon *55*, 1869–1887.

Renaud, G., Slon, V., Duggan, A.T., and Kelso, J. (2015). Schmutzi: estimation of contamination and mitochondrial consensus calling for ancient DNA. Genome Biol. *16*, 224.

Rohland, N., and Hofreiter, M. (2007). Ancient DNA extraction from bones and teeth. Nat. Protoc. *2*, 1756–1762.

Cell
Article

Rohland, N., Harney, E., Mallick, S., Nordenfelt, S., and Reich, D. (2015). Partial uracil-DNA-glycosylase treatment for screening of ancient DNA. Philos. Trans. R. Soc. Lond. B Biol. Sci. 370, 20130624.

Rokita, E., Hermes, C., Nolting, H.-F., and Ryczek, J. (1993). Substitution of calcium by strontium within selected calcium phosphates. J. Cryst. Growth 130, 543–552.

Saag, L., Varul, L., Scheib, C.L., Stenderup, J., Allentoft, M.E., Saag, L., Pagani, L., Reidla, M., Tambets, K., Metspalu, E., et al. (2017). Extensive Farming in Estonia Started through a Sex-Biased Migration from the Steppe. Curr. Biol. 27, 2185–2193.

Scheib, C.L., Li, H., Desai, T., Link, V., Kendall, C., Dewar, G., Griffith, P.W., Mörseburg, A., Johnson, J.R., Potter, A., et al. (2018). Ancient human parallel lineages within North America contributed to a coastal expansion. Science 360, 1024–1027.

Schubert, M., Lindgreen, S., and Orlando, L. (2016). AdapterRemoval v2: rapid adapter trimming, identification, and read merging. BMC Res. Notes 9, 88.

Schuenemann, V.J., Bos, K., DeWitte, S., Schmedes, S., Jamieson, J., Mittnik, A., Forrest, S., Coombes, B.K., Wood, J.W., Earn, D.J.D., et al. (2011). Targeted enrichment of ancient pathogens yielding the pPCP1 plasmid of Yersinia pestis from victims of the Black Death. Proc. Natl. Acad. Sci. USA 108, E746–E752.

Schulting, R.J., Ramsey, C.B., Bazaliiskii, V.I., Goriunov, O.I., and Weber, A. (2014). Freshwater Reservoir Offsets Investigated Through Paired Human-Faunal 14C Dating and Stable Carbon and Nitrogen Isotope Analysis at Lake Baikal, Siberia. Radiocarbon 56, 991–1008.

Schulting, R.J., Bronk Ramsey, C., Bazaliiskii, V.I., and Weber, A. (2015). Highly Variable Freshwater Reservoir Offsets Found along the Upper Lena Watershed, Cis-Baikal, Southeast Siberia. Radiocarbon 57, 581–593.

Sealy, J.C., van der Merwe, N.J., Thorp, J.A.L., and Lanham, J.L. (1987). Nitrogen isotopic ecology in southern Africa: Implications for environmental and dietary tracing. Geochim. Cosmochim. Acta 51, 2707–2717.

Sikora, M., Pitulko, V.V., Sousa, V.C., Allentoft, M.E., Vinner, L., Rasmussen, S., Margaryan, A., de Barros Damgaard, P., de la Fuente, C., Renaud, G., et al. (2019). The population history of northeastern Siberia since the Pleistocene. Nature 570, 182–188.

Siska, V., Jones, E.R., Jeon, S., Bhak, Y., Kim, H.-M., Cho, Y.S., Kim, H., Lee, K., Veselovskaya, E., Balueva, T., et al. (2017). Genome-wide data from two early Neolithic East Asian individuals dating to 7700 years ago. Sci. Adv. 3, e1601877.

Smith, B.N., and Epstein, S. (1971). Two categories of c/c ratios for higher plants. Plant Physiol. 47, 380–384.

Spiliopoulou, A., Colombo, M., Orchard, P., Agakov, F., and McKeigue, P. (2017). GeneImp: Fast imputation to large reference panels using genotype likelihoods from ultralow coverage sequencing. Genetics 206, 91–104.

Spyrou, M.A., Tukhbatova, R.I., Feldman, M., Drath, J., Kacki, S., Beltrán de Heredia, J., Arnold, S., Sitdikov, A.G., Castex, D., Wahl, J., et al. (2016). Historical Y. pestis genomes reveal the European Black Death as the source of ancient and modern plague pandemics. Cell Host & Microbe 19, 874–881.

Spyrou, M.A., Tukhbatova, R.I., Wang, C.-C., Valtueña, A.A., Lankapalli, A.K., Kondrashin, V.V., Tsybin, V.A., Khokhlov, A., Kühnert, D., Herbig, A., et al. (2018). Analysis of 3800-year-old Yersinia pestis genomes suggests Bronze Age origin for bubonic plague. Nat. Commun. 9, 2234.

Spyrou, M.A., Keller, M., Tukhbatova, R.I., Scheib, C.L., Nelson, E.A., Andrades Valtueña, A., Neumann, G.U., Walker, D., Alterauge, A., Carty, N., et al. (2019). Phylogeography of the second plague pandemic revealed through analysis of historical Yersinia pestis genomes. Nat. Commun. 10, 4470.

Stamatakis, A. (2014). RAxML version 8: a tool for phylogenetic analysis and post-analysis of large phylogenies. Bioinformatics 30, 1312–1313.

Sun, Y.-C., Jarrett, C.O., Bosio, C.F., and Hinnebusch, B.J. (2014). Retracing the evolutionary path that led to flea-borne transmission of Yersinia pestis. Cell Host Microbe 15, 578–586.

Tashak, V.I. (2000). Tortsovye klinovidnye nukleusy Zapadnogo Zabaikaliya v pozdnem paleolite i mezolite. In Kamennyi Vek Yuzhnoi Sibiri i Mongolii: Teoreticheskie Problemy I Novye Otkrytiya (Buryat scientific center SB RAS), pp. 59–74.

Tashak, V.I. (2005). Paleoliticheskie i mezoliticheskie pamiatniki Ust'-Kiakhty (Buryatia Scientific Center of the Siberian Branch of the Russian Academy of Sciences).

Tavaré, S. (1986). Some probabilistic and statistical problems in the analysis of DNA sequences. Lect. Math Life Sci. 17, 57–86.

Thorvaldsdóttir, H., Robinson, J.T., and Mesirov, J.P. (2013). Integrative Genomics Viewer (IGV): high-performance genomics data visualization and exploration. Brief. Bioinform. 14, 178–192.

Vågene, Å.J., Herbig, A., Campana, M.G., Robles García, N.M., Warinner, C., Sabin, S., Spyrou, M.A., Andrades Valtueña, A., Huson, D., Tuross, N., et al. (2018). Salmonella enterica genomes from victims of a major sixteenth-century epidemic in Mexico. Nat. Ecol. Evol. 2, 520–528.

Vlast'truda (1928). 21 oktyabrya. 246, 4.

Vlast'truda (1929). 28 iyulya. 17, 4.

Wang, C.C., Reinhold, S., Kalmykov, A., Wissgott, A., Brandt, G., Jeong, C., Cheronet, O., Ferry, M., Harney, E., Keating, D., et al. (2019). Ancient human genome-wide data from a 3000-year interval in the Caucasus corresponds with eco-geographic regions. Nat. Commun. 10, 590.

Weber, A. (1995). The neolithic and early bronze age of the Lake Baikal Region: A review of recent research. J. World Prehist. 9, 99–165.

Weber, A.W., and Bettinger, R. (2010). Middle Holocene hunter-gatherers of Cis-Baikal, Siberia: An overview for the new century. J. Anthropol. Archaeol. 29, 491–506.

Weber, A.W., Link, D.W., and Katzenberg, M.A. (2002). Hunter-gatherer culture change and continuity in the middle holocene of the Cis-Baikal, Siberia. J. Anthropol. Archaeol. 21, 230–299.

Weber, A.W., Beukens, R.P., Bazaliiskii, V.I., Goriunova, O.I., and Savel'ev, N.A. (2006). Radiocarbon Dates from Neolithic and Bronze Age Hunter-Gatherer Cemeteries in the Cis-Baikal Region of Siberia. Radiocarbon 48, 127–166.

Weber, A.W., Schulting, R.J., Bronk Ramsey, C., Bazaliiskii, V.I., Goriunova, O.I., and Berdnikova, N.E. (2016). Chronology of middle Holocene hunter–gatherers in the Cis-Baikal region of Siberia: Corrections based on examination of the freshwater reservoir effect. Quat. Int. 419, 74–98.

Wickham, H. (2016). ggplot2: Elegant Graphics For Data Analysis (Springer).

Zhgenti, E., Johnson, S.L., Davenport, K.W., Chanturia, G., Daligault, H.E., Chain, P.S., and Nikolich, M.P. (2015). Genome Assemblies for 11 Yersinia pestis Strains Isolated in the Caucasus Region. Genome Announc. 3, 3.

Zhou, D., and Yang, R. (2009). Molecular Darwinian evolution of virulence in Yersinia pestis. Infect. Immun. 77, 2242–2250.

Zimbler, D.L., Schroeder, J.A., Eddy, J.L., and Lathem, W.W. (2015). Early emergence of Yersinia pestis as a severe respiratory pathogen. Nat. Commun. 6, 7487.

Zotkina, L.V., Pavlenok, G.D., and Tashak, V.I. (2018). Tekhnologiya proizvodstva busin iz skorlupy yaic strausa v final'nom paleolite Zapadnogo Zabajkal'ya [Technology of Ostrich Eggshell Bead Production in the Final Palaeolithic of Western Transbaikalia]. Strat. plus. Archaeol. Cult. Anthropol. 1, 181–197.

Zubkov, V.S. (2010). Materialy iz drevnih mogil s territorii poselka Kachug i u derevni SHishkino na Verhnej Lene (raskopki A. P. Okladnikova 1928-1930, 1941 gg.). Izv. Lab. Drevnih Tekhnologij. Irkutsk Izd-vo IrGTU. 8, 135–146.

Cell
Article

CellPress

STAR★METHODS

KEY RESOURCES TABLE

REAGENT or RESOURCE	SOURCE	IDENTIFIER
Biological Samples		
Ancient skeletal element	This study	ANG001
Ancient skeletal element	This study	BZK002
Ancient skeletal element	This study	GLZ001
Ancient skeletal element	This study	GLZ002
Ancient skeletal element	This study	GLZ003
Ancient skeletal element	This study	IUO001
Ancient skeletal element	This study	KAG001
Ancient skeletal element	This study	KAG002
Ancient skeletal element	This study	KPT001
Ancient skeletal element	This study	KPT002
Ancient skeletal element	This study	KPT003
Ancient skeletal element	This study	KPT004
Ancient skeletal element	This study	KPT005
Ancient skeletal element	This study	KPT006
Ancient skeletal element	This study	STB001
Ancient skeletal element	This study	STB002
Ancient skeletal element	This study	ZPL001
Ancient skeletal element	This study	ZPL002
Ancient skeletal element	This study	UKY001
Chemicals, Peptides, and Recombinant Proteins		
D1000 ScreenTapes	Agilent Technologies	Cat# 5067-5582
D1000 Reagents	Agilent Technologies	Cat# 5067-5583
PfuTurbo Cx Hotstart DNA Polymerase	Agilent Technologies	Cat# 600412
Herculase II Fusion DNA Polymerase	Agilent Technologies	Cat# 600679
1x Tris-EDTA pH 8.0	AppliChem	Cat# A8569,0500
Sodiumhydroxide Pellets	Fisher Scientific	Cat# 10306200
Sera-Mag Magnetic Speed-beads Carboxylate-Modified (1 mm, 3EDAC/PA5)	GE LifeScience	Cat# 65152105050250
0.5 M EDTA pH 8.0	Life Technologies	Cat# AM9261
10x Buffer Tango	Life Technologies	Cat# BY5
GeneRuler Ultra Low Range DNA Ladder	Life Technologies	Cat# SM1211
Isopropanol	Merck	Cat# 1070222511
Ethanol	Merck	Cat# 1009832511
USER enzyme	New England Biolabs	Cat# M5505
Uracil Glycosylase inhibitor (UGI)	New England Biolabs	Cat# M0281
Bst DNA Polymerase2.0, large frag.	New England Biolabs	Cat# M0537
BSA 20mg/mL	New England Biolabs	Cat# B9000
T4 Polynucleotide Kinase	New England Biolabs	Cat# M0201
T4 DNA Polymerase	New England Biolabs	Cat# M0203
PEG-8000	Promega	Cat# V3011
20% SDS	Serva	Cat# 39575.01
Proteinase K	Sigma Aldrich	Cat# P2308

(Continued on next page)

Continued

REAGENT or RESOURCE	SOURCE	IDENTIFIER
Guanidine hydrochloride	Sigma Aldrich	Cat# G3272
3M Sodium Acetate (pH 5.2)	Sigma Aldrich	Cat# S7899
Water	Sigma Aldrich	Cat# 34877
Tween-20	Sigma Aldrich	Cat# P9416
5M NaCl	Sigma Aldrich	Cat# S5150
Denhardt's solution	Sigma Aldrich	Cat# D9905
ATP 100 mM	Thermo Fisher Scientific	Cat# R0441
1 M Tris-HCl pH 8.0	Thermo Fisher Scientific	Cat# 15568025
dNTP Mix	Thermo Fisher Scientific	Cat# R1121
SSC Buffer (20x)	Thermo Fisher Scientific	Cat# AM9770
GeneAmp 10x PCR Gold Buffer	Thermo Fisher Scientific	Cat# 4379874
Dynabeads MyOne Streptavidin T1	Thermo Fisher Scientific	Cat# 65602
Salmon sperm DNA	Thermo Fisher Scientific	Cat# 15632-011
Human Cot-I DNA	Thermo Fisher Scientific	Cat#15279011
0.5M HCl	Carl Roth	Cat# 9277.1
HNO_3	Merck	Cat# 1.00456.2500
Critical Commercial Assays		
High Pure Viral Nucleic Acid Large Volume Kit	Roche	Cat# 5114403001
HiSeq 4000 SBS Kit (50/75 cycles)	Illumina	Cat# FC-410-1001/2
DyNAmo Flash SYBR Green qPCR Kit	Thermo Fisher Scientific	Cat# F415L
MinElute PCR Purification Kit	QIAGEN	Cat# 28006
Quick Ligation Kit	New England Biolabs	Cat# M2200L
Oligo aCGH/Chip-on-Chip Hybridization Kit	Agilent Technologies	Cat# 5188-5220
Deposited Data		
Raw and analyzed data (European nucleotide archive)	This study	ENA: PRJEB37007
1240K Genotype data (Edmond Data Repository of Max Planck Society)	This study	https://edmond.mpdl.mpg.de/imeji/collection/z9C4DN1vFlqsmbHO
Software and Algorithms		
EAGER 1.92.55	Peltzer et al., 2016	https://eager.readthedocs.io/en/latest/
AdapterRemoval 2.2.0	Schubert et al., 2016	https://github.com/MikkelSchubert/adapterremoval
BWA 0.7.12	Li and Durbin, 2009	http://bio-bwa.sourceforge.net/
DeDup 0.12.1	Peltzer et al., 2016	https://github.com/apeltzer/DeDup
mapDamage 2.0.6	Jónsson et al., 2013	https://github.com/ginolhac/mapDamage
bamUtil 1.0.13	https://github.com/statgen/bamUtil	https://github.com/statgen/bamUtil
CircularMapper	Peltzer et al., 2016	https://github.com/apeltzer/CircularMapper
Schmutzi	Renaud et al., 2015	https://github.com/grenaud/schmutzi
SAMtools 1.3	Li et al., 2009	http://www.htslib.org/doc/samtools.html
pileupCaller	https://github.com/stschiff/sequenceTools	https://github.com/stschiff/sequenceTools
GATK 3.5	DePristo et al., 2011	https://gatk.broadinstitute.org/hc/en-us
GeneImp 1.4	Spiliopoulou et al., 2017	https://pm2.phs.ed.ac.uk/geneimp/
SHAPEIT v2.r837	Delaneau et al., 2013	https://mathgen.stats.ox.ac.uk/genetics_software/shapeit/shapeit.html
yHaplo	Poznik, 2016	https://github.com/23andMe/yhaplo
ANGSD 0.910	Korneliussen et al., 2014	http://www.popgen.dk/angsd/index.php/ANGSD

Cell
Article

CellPress

Continued

REAGENT or RESOURCE	SOURCE	IDENTIFIER
EIGENSOFT 6.0.1	Patterson et al., 2006	https://github.com/DReichLab/EIG
ADMIXTURE 1.3.0	Alexander et al., 2009	http://software.genetics.ucla.edu/admixture/
PLINK v1.90b3.29	Purcell et al., 2007	http://www.cog-genomics.org/plink2/
BEAGLE v4.1	Browning and Browning, 2013	https://faculty.washington.edu/browning/beagle/b4_1.html
ADMIXTOOLS 5.1	Patterson et al., 2012	https://github.com/DReichLab/AdmixTools
DATES 763	Moorjani and Patterson, 2018	https://github.com/priyamoorjani/DATES
MALT 0.4.0	Vågene et al., 2018	https://github.com/husonlab/malt
HOPS	Hübler et al., 2019	https://github.com/rhuebler/HOPS
picard MarkDuplicates 1.1.40	http://broadinstitute.github.io/picard/	http://broadinstitute.github.io/picard/
MultiVCFAnalyzer v0.85	https://github.com/alexherbig/MultiVCFAnalyzer	https://github.com/alexherbig/MultiVCFAnalyzer
RaxML 8.2.9	Stamatakis, 2014	https://cme.h-its.org/exelixis/web/software/raxml/index.html
TempEst v1.5	http://tree.bio.ed.ac.uk/software/tempest/	http://tree.bio.ed.ac.uk/software/tempest/
BEAST v1.8	Drummond and Rambaut, 2007	http://beast.community/
Tracer v1.6	http://tree.bio.ed.ac.uk/software/tracer	http://tree.bio.ed.ac.uk/software/tracer/

RESOURCE AVAILABILITY

Lead Contact
Further information and requests for resources and reagents should be directed to and will be fulfilled by the Lead Contact, Johannes Krause (krause@shh.mpg.de).

Materials Availability
This study did not generate new unique reagents.

Data and Code Availability
Aligned reads to the human reference genome and mtDNA from the 19 newly reported ancient individuals and the *Y. pestis* capture sequencing reads of two individuals are available at the ENA archive under the accession number PRJEB37007. Haploid genotype data for the 1240K panel are available in the eigenstrat format at the Edmond Data Repository of Max Planck Society (https://edmond.mpdl.mpg.de/imeji/collection/z9C4DN1vFlqsmbHO)

EXPERIMENTAL MODEL AND SUBJECT DETAILS

Archaeological information
In this study we collected 7 petrous bones and 13 teeth from 19 individuals excavated from 10 different sites, including one Ust-Kyakhta-3 site from the south of Lake Baikal and the other nine sites in *cis*-Baikal region.
Sample from the Western Trans-Baikal
Ust-Kyakhta-3 Site.
- UKY001, tooth fragment (Ust'Kyakhta-3 1976 Excavation area 1 Layer 1 Square B-3)

The stratified Ust-Kyakhta-3 site is located on the right bank of the Selenga River in the vicinity of Ust-Kyakhta village in the Kyakhtinski Region of the Republic of Buryatia (Russian Federation). The site was discovered in 1947 by an archaeological team led by Academician A. P. Okladnikov. Initial excavations at Ust-Kyakhta-3 were carried out in 1976 and 1978, revealing two culture-bearing horizons. More than 40,000 stone artifacts were recovered; abundant faunal remains were also collected (Okladnikov, 1977, 1979).

Archaeological work undertaken at the site in 2012 (Pavlenok, 2015a) yielded two human tooth fragments among archaeological materials collected in the course of sieving the sediments of Layer 1 (Pavlenok et al., 2019).

Excavations at Ust-Kyakhta-3 in 2012 provided additional information on the stratigraphy of the site. The stratigraphic column was subdivided into 12 lithological strata. Strata from 1 to 5 represent diluvial and aeolian sediments. The lower segment of the column, including Strata 6 through 12, was formed by flood-plain alluvium. Archaeological materials were noted in association with two

lithological strata. Archaeological Layer 1 is enclosed within lithological Stratum 9, comprising a humus-containing fine-grained sandy loam from 4 to 12 cm thick. Archaeological Layer 2 is associated with lithological Stratum 11, composed of light brown sandy loam from 15 to 20 cm thick.

Cultural remains associated with Ust-Kyakhta-3 Layer 1 were accumulated during the terminal Pleistocene with associated dates of 14,165 ± 236 – 14,183 ± 234 cal BP. Archaeological materials from Layer 2 yielded similar dates ranging from 13,758 ± 138 – 14,326 ± 266 cal BP (calibration was carried out following http://www.calpal-online.de/) (Pavlenok et al., 2019).

The lithic industry is characterized by flaking technology of typical wedge-shaped cores aimed at the production of micro-blades; blades were produced through flaking flat and sub-prismatic cores. The archaeological assemblage from Layer 1 is larger and contains a greater variety of various typologically and technologically significant artifacts. All the major inferences concerning stone reduction at Ust-Kyakhta-3 are based on the collection from Layer 1. The materials from Layer 2 do not contradict these inferences. One specific feature of this culture is a special strategy of core reduction. Upon exhaustion of the flaking surface, some flat cores were modified into blanks for wedge-shaped cores together with pebbles and thick spalls. Two modification strategies were reconstructed (Pavlenok, 2015b; Tashak, 2000). Analyses of the tool kit have shown that the targets of primary reduction; blades and micro-blades; were primarily selected for secondary working. The tool kit is dominated by knives, side- and end-scrapers and specific Ust-Kyakhta points (Tashak, 2005); burins fashioned mostly on blades are less numerous. Borers made on micro-blades (Pavlenok, 2015a) constitute a characteristic series in the tool kit.

In addition to lithic artifacts, bone implements were also recovered, including points, awls, needles, hafts of composite tools with one or two cutting edges, fishhooks (Pavlenok, 2014; Tashak, 2005), and a series of ostrich eggshell beads (Zotkina et al., 2018).

Analytical data from the Ust-Kyakhta-3 archaeological collection provide solid evidence for their attribution to the Selenga Terminal Paleolithic culture (Pavlenok, 2015a). The origin of this culture is associated with older, autochthonous complexes in Trans-Baikalia.

Individuals from the cis-Baikal region

These human remains are currently housed in the Research Institute and Museum of Anthropology (RIMA) of the Lomonosov Moscow State University (MSU). Most of these remains were collected by Alexey Okladnikov during his first few independent archaeological excavations as an employee of the Irkutsk museum of regional studies between 1926 and 1929 in the Verkholenski and Irkutski uyezds of the Irkutsk Governorate. Now these territories form several districts of the East Siberian region. The works were regularly reported by the local press, informing general public not only about the archaeological excavations, but also about the establishment of a special department in the Irkutsk museum of regional studies to store the excavation materials, as well as the establishment of the District committee for the protection of the Paleo-Ethnological heritage of the region (Vlast'truda, 1928).

In 1926 Okladnikov documented about ten Late Stone Age dwelling sites in the Verkholenski uyezd, and he also discovered a Neolithic cemetery nearby Iushino village (Okladnikov, 1926). During 1927 an archaeological exploration took place in Kachugsky District along the Lena river tributaries, including Biryulka, Anga, Manzurka and some other rivers. As a result, several Neolithic dwelling sites were discovered as well as a cemetery in Khaptsagai area near Bayraki village on the right bank of the Manzurka river (Okladnikov, 1928, 1929). One month prior to this, local press distributed an information about excavations in the vicinities of the Stepno-Baltaiskii ulus, by Okladnikov and Kveiko, resulting in the discovery of human remains, stone scrapers, polished green nephrite knife, bone ornaments and more (Vlast'truda, 1929). The same year Okladnikov conducted archaeological excavations near Zapleskino village in the Zhigalovsky District. The resulting findings were also transferred to the Irkutsk museum of regional studies.

In 1929 most of the anthropological materials from Okladnikov's excavations were transferred to the Anthropological museum of the Lomonosov Moscow State University.

Through the work of several generations of Russian specialists (N.I. Vitkovsky, M.P. Ovchinnikov, G.F. Debets, A.P. Okladnikov, M.M. Gerasimov, L.P., L.P. Chlobystin and others), characteristic archaeological cultures of the Neolithic and the Early Bonze Age of the Cisbaikalia were defined. Over the past decades, the chronology and periodization of the Neolithic and the Bronze Age of the Cisbaikalia were refined (Bazalijskij, 2012; Mamonova and Sulerzhickij, 1989, 2008; Weber et al., 2002, 2006). As a result, two clusters of the Early Neolithic (EN) sites and a multicomponent cluster of the Late Neolithic and Early Bronze Age (LN-EBA) sites were defined. The first Early Neolithic group includes sites of the Kitoi mortuary tradition, represented by large well-known cemeteries in South Angara region of Southern Baikal, such as the Shamanka II cemetery. The second cluster of the Early Neolithic sites is located at adjacent regions in the Upper Lena River, Olkhon and Western Transbaikal area, different from the Kitoi group mainly in artifact composition and mortuary tradition. This cluster is represented by several small cemeteries and few burials (Movsesian et al., 2015). The EN groups practiced hunting, fishing and sealing, with large and unevenly distributed population, differential mobility and substantial social differentiation. The LN-EBA (Serovo-Isakovo-Glazkovo) cultures are represented by various local variants spread over large territory. Similar with EN population, they had formal cemeteries, practiced hunting, fishing and sealing, but are represented by larger and evenly distributed populations that had moderate mobility and social differentiation (Weber and Bettinger, 2010).

Earlier craniometric studies by Russian anthropologist Debets suggested that the EN and the LN-EBA populations were genetically distinct (Debets, 1930, 1948). Mamonova shown that while differences between Serovo and Glazkovo craniological samples were minor, Kitoi crania differed substantially from both of these samples, and the extent of the difference between Kitoi and Serovo crania was greater than between Kitoi and Glazkovo crania (Mamonova, 1973). It is likely that Serovo and Glazkovo series represent single craniological complex with local variants. Overall, this is the same craniological complex present in Angara (Alekseev and Mamonova, 1979).

Cell
Article

CellPress

Recent craniometric studies as well as studies of non-metric cranial traits suggest that the Early Neolithic Kitoi groups and the Late Neolithic Serovo groups belong to different gene pools. However, at the same time similarities were found between the Kitoi group from Angara region and chronologically distant Bronze Age Glazkovo groups from Angara, Upper Lena and Transbaikal territories. It is hypothesized that the morphological diversity of Glazkovo groups could be due to their mixture with the descendants of the Kitoi groups who left the Cisbaikalia and later migrated back from the neighboring territories. It is assumed that the population of the Transbaikalia, which exhibited extremely stable anthropological profile from the Early Neolithic to the Bronze Age time period, penetrated Cisbaikalia during the Glazkovo stage and influenced the formation of the Early Bronze Age population's gene pool (Movsesian et al., 2014, 2015).

Five skulls (RIMA number 4620 and 4571) were donated to the Anthropological museum of the MSU in 1885 by Siberian archaeologist I.T. Savenkov. In 1884 he conducted archaeological research in the villages: Ladeyka, Nyasha, Bazaikha and Sobakino (Krasnoyarsk district).

Angara Site.

- ANG001, tooth M3 lower right (RIMA number 4620)

Savenkov found this cranium while excavating ancient graves on the banks of Angara River. No archaeological context is available.

Bazaikha Site.

- BZK002, tooth M2 lower right (RIMA number 4571)

Savenkov found two skulls near the river Bazaikha on the right banks of Yenisei river in Krasnoyarsk district. No archaeological context is available. According to Okladnikov (1950), the skeletal remains may be attributed to the Bronze Age Karasuk culture between late second to early first millennium BC, based on the archaeological findings described by Savenkov.

Glazkovskoe Predmestie Site.

- GLZ001, tooth M2 upper left, (RIMA number 4616),
- GLZ002, tooth M2 upper right, (RIMA number 4617),
- GLZ003, tooth M1 lower right, (RIMA number 4618)

Archaeological and anthropological findings were from the Glazkovo outskirts of Irkutsk city found during excavations for the foundation of a new infant asylum. Construction works were conducted under the lead of V.P. Sukachov from the summer of 1887. An ancient burial was discovered in the autumn of the same year. N.I. Vitkovski, an employee of the museum of the East Siberian division of the Russian Geographical society, was called in upon discovery. This researcher was known for his excavations on the Kitoi cemetery between 1880-1881 that gave the name to the Early Neolithic culture of the region. By the time Vitkovski arrived at the site, construction workers had destroyed the burials. He collected six crania and a few artifacts, including two rings made from white nephrite. According to several eyewitnesses, the interred individuals were in the sitting position, facing East. Under Vitkovski's supervision, excavation continued and an undamaged burial was discovered. The skeleton was in flexed position with the legs bent at the knees. Two perforated pendants from cleaved wild boar tusk were found on the cranium. The findings were transported to the museum of the Russian Geographical society's division (Debets, 1930). Among these, three crania were later transferred to the MSU and became part of its osteological collections.

Iushino Site.

- IUO001, part of left *os temporale* (*pars petrosa*), (RIMA number 8311)

In 1926 Okladnikov discovered a Neolithic burial ground near Iushino village (Okladnikov, 1926). Human skeletal remains and artifacts from three burials were transferred to the Irkutsk museum. Based on these, the remains are attributed to the Early Neolithic period of the Kitoi culture (Alekseev and Mamonova, 1979). The cranium from the Grave 3 was later transferred to the MSU.

Kachug Site.

- KAG001, part of left *os temporale* (*pars petrosa*), (RIMA number 8307)
- KAG002, tooth M1 lower left, (RIMA number 8308)

The Kachug burial ground was located on the right bank of the Lena river, above the Kachug village. Currently, the exact location of this burial ground cannot be identified. Here in 1927 three burials were excavated, dated to the Eneolithic time (Okladnikov, 1955). Skeletal remains from the grave 2 (# 8307) and grave 3 (# 8308) were transferred to the Anthropological museum. Grave 2 (# 8307) contained polished nephrite ring and a black stone disc (Okladnikov, 1955). From grave 3 (# 8308) Okladnikov described the following artifacts: a small copper or bronze knife "firmly attached to the massive horn handle," "this knife is flat, with double edged blade, its protruding part has triangular outline," and two copper tubes (Okladnikov, 1955). Items found in these burials have analogies in well-documented and dated burial complexes of Angara, Upper Lena and Olkhon areas, attributed to the Glazkovo culture of the Late Neolithic – Early Bronze Age (Alekseev and Mamonova, 1979; Zubkov, 2010).

Khaptsagai Site.

- KPT001, part of left *os temporale* (*pars petrosa*), (RIMA number 8313),
- KPT002, part of left *os temporale* (*pars petrosa*), (RIMA number 8300),
- KPT003, M2 upper right, (RIMA number 8302),

- KPT004, M2 upper left, (RIMA number 8304),
- KPT005, M2 lower right, (RIMA number 8301),
- KPT006, M1 lower left, (RIMA number 8305)

In 1927 an archaeological exploration in Kachug area took place. As a result, several Neolithic dwelling sites were discovered and a burial ground in Khaptsagay area near Bayraki village, on the right bank of Manzurka river (Okladnikov, 1928). Twenty ancient burials were excavated. Skeletal remains from six graves were transferred to the Anthropological museum: from grave 7 (inventory #8300), grave 12 (#8304), grave 13 (#8305), grave 14 (#8302), grave 19 (#8301) and from a looted grave (#8313). Some of the individuals were in a flexed position within the interment, under a stone vault. Numerous artifacts were unearthed such as white nephrite rings, green nephrite knives, stone arrow heads and spear points, stone chisel, awls and stone needles in ornamented needle cases (Okladnikov, 1929). According to the researchers, human skeletal remains are dated to the Glazkovo stage of the Late Neolithic based on the artifacts (Alekseev and Mamonova, 1979).

Zhigalovo Site.
- STB001, part of right *os temporale (pars petrosa)*, (RIMA number 8315)

This cranium has an abbreviation "Zh. 1" written on it, which likely stands for Zhigalovo, grave 1, where the cranium was presumably discovered. Based on the finding date (year 1929) this may be a cranium from a disintegrated grave, discovered by Okladnikov on the Lena river bank on the opposite side of the Zhigalovo village, the district center. The grave was severely destroyed due to displacement and erosion of clay layers of the ancient terrace. Here, stone bow plates attributed to Late Neolithic Serovo culture were discovered. This was the first finding of the bow remnants from this period (Okladnikov, 1950).

Stepno-Baltaiskii ulus Site.
- STB002, part of left *os temporale (pars petrosa)*, (RIMA number 8314)

Okladnikov and Kveiko found Stone Age burials in the vicinity of the Stepno-Baltaiskii ulus. Stone scrapers, a polished green jade knife, bone ornaments and patterned sawn elk shoulder blades were found within these burials (Vlast'truda, 1929). The skeletal remains (the cranium and postcranial skeleton) from the grave 1 were transferred to the Anthropological museum of the MSU. According to the researcher, this skeleton may belong to the Early Neolithic period of the Kitoi culture (Alekseev and Mamonova, 1979).

Zapleskino Site.
- ZPL001, part of left *os temporale (pars petrosa)*, (RIMA number 8309),
- ZPL002, M2 lower right, (RIMA number 8310)

These remains are from burials in the vicinity of Zapleskino village in the Zhigalovsky District. Okladnikov transferred two crania to the Anthropological museum, including crania from grave 1 (#8309) and grave 4 (#8310). These findings are dated to the Late Neolithic – Early Bronze Age stage of the Glazkovo culture (Alekseev and Mamonova, 1979).

METHOD DETAILS

Radiocarbon dating and calibration
Except for UKY001, all the other 19 samples were analyzed by accelerator mass spectrometry (AMS) at Manheim (MAMS). For UKY001 we used the three published ^{14}C dates of charcoal and bone materials from the same layer reported as references of the sample age (Orlova, 1995; Pavlenok et al., 2019), and combined them in calibration. All the radiocarbon dates were calibrated using the dataset IntCal 13 (Reimer et al., 2013). Prior to conversion to a calendar age it was important to determine whether there were any dietary offsets that could influence the calibrated ages, as freshwater reservoir effects, including those from the Lake Baikal region, are known to make radiocarbon ages appear as much as > 1,000 years in some systems (Nomokonova et al., 2013; Ramsey et al., 2014; Schulting et al., 2014, 2015). We used stable carbon (δ^{13}C) and nitrogen (δ^{15}N) measurements of bone collagen from the same individuals, as well as published regression equations to estimate the offset between conventional and terrestrial radiocarbon dates (Schulting et al., 2014, 2015). The estimated offsets are given in Table S1.

Stable isotope analysis
Background
δ^{13}C variability in terrestrial ecosystems is primarily driven by plants that variously utilize two dominant photosynthetic pathways, C_3 and C_4 (Smith and Epstein, 1971). C_3 plants, including virtually all trees, shrubs, and temperate grasses, and domesticates such as wheat and barley, have values from *c.* -24 to $-36‰$ (global mean $-26.5‰$). C_4 plants, including domesticated grasses such as millet, have values ranging from *c.* -9 to $-17‰$ (global mean $-12‰$ (Smith and Epstein, 1971). These non-overlapping distinctions are reflected in the tissues of consumers (Ambrose and Norr, 1993). δ^{15}N varies with trophic level, and δ^{15}N trophic shifts of $+2$-$6‰$ being documented in terrestrial ecosystems (Deniro and Epstein, 1981; Sealy et al., 1987). The long length of aquatic foodchains, leads to distinctively high δ^{15}N in consumers (Minagawa and Wada, 1984). However, while marine consumers have both high δ^{13}C and δ^{15}N, δ^{13}C is less predictable in freshwater ecosystems necessitating detailed baseline reconstruction (Katzenberg and Weber, 1999; Kiyashko et al., 1998). δ^{13}C and δ^{15}N analysis of human bone collagen primarily determines the isotopic values of the protein input

to the diet, with a much more minor contribution of lipid and carbohydrate sources (Ambrose and Norr, 1993). This means that the $\delta^{13}C$ and $\delta^{15}N$ values of bone and dentine collagen will be heavily affected by foods that are high in protein (Ambrose and Norr, 1993). In addition, tooth dentine forming during a period of breastfeeding (e.g., permanent M1) will be elevated in $\delta^{15}N$ to appear a whole trophic level higher (Fuller et al., 2003). The same may also apply to certain portions of the skull including the petrus (Jørkov et al., 2009).

Stable isotope analysis

We sampled the petrous bones of seven individuals and tooth dentine of 12 individuals (Table S1) for stable carbon and nitrogen isotope analysis in order to determine differences in diet and the potential impact of the reservoir effect on the ages of individuals analyzed.

We obtained c. 0.5 g of dentine or bone powder using a handheld Dremel drill. All specimens were first cleaned using abrasion by sandblaster. We extracted collagen from the resulting powder using a modified Longin methodology (Longin, 1971). Samples were demineralised by immersion in 0.5M HCl for 1-7 days. Once demineralisation was complete, samples were rinsed three times with ultra-pure H_2O. The residue was gelatinized in pH3 HCl at $70°C$ for 48 hours and Ezee-filters were used to remove the insoluble residues from the soluble collagen solution (Brock et al., 2013). Samples were lyophilized for 48hrs. 1.0 mg of the resulting purified collagen was weighed in duplicates into tin capsules for analysis.

The $\delta^{13}C$ and $\delta^{15}N$ ratios of the weighed-out bone collagen were measured using a Thermo Scientific Flash 2000 Elemental Analyzer coupled to a Thermo Delta V Advantage Isotope Ratio Mass Spectrometer at the Stable Isotope Laboratory of the Department of Archaeology, Max Planck Institute for the Science of Human History, Jena. Values are reported as the ratio of the heavier isotope to the lighter isotope ($^{13}C/^{12}C$ or $^{15}N/^{14}N$) as δ values in parts per mill (‰) relative to international standards, VPDB for $\delta^{13}C$ and atmospheric N2 (AIR) for $\delta^{15}N$. The results reported for the samples were calibrated against international standards of (IAEA-CH-6: $\delta^{13}C = -10.80 \pm 0.47$ ‰, IAEA-N-2: $\delta^{15}N = 20.3 \pm 0.2$ ‰, and USGS40: $\delta^{13}C = -26.38 \pm 0.042$ ‰, $\delta^{15}N = 4.5 \pm 0.1$ ‰). Machine error was determined using repeat runs of a laboratory standard (fish gelatin: $\delta^{13}C = \sim-15.1$ ‰, $\delta^{15}N = \sim14.3$ ‰). Based on replicate analyses machine error over the course of a year is ± 0.2‰ for $\delta^{13}C$ and ± 0.2‰ for $\delta^{15}N$. Overall measurement precision was studied through the measurement of repeats of fish gelatin (n = 80, ± 0.2‰ for $\delta^{13}C$ and ± 0.2‰ for $\delta^{15}N$).

The resulting $\delta^{13}C$ and $\delta^{15}N$ values were used to independently estimate the potential impacts on the 'reservoir effect' of radiocarbon ages from the skeletons caused by the consumption of freshwater fish in the Lena River and Angara River regions. There has been a long history of research into the 'reservoir' effects of prehistoric individuals living in this region based on the paired radiocarbon dating of human bone and associated animal remains from the same graves, and correlations have been found between the extent of the offset in radiocarbon (^{14}C) years and human stable isotope values (Ramsey et al., 2014; Schulting et al., 2014, 2015). Here, we used established equations from Schulting et al. (2014, 2015) to estimate the radiocarbon offset based on our data. For individuals from the Lena River we have used Schulting et al.'s (2015, Table 3 pp. 586) "Full data set, $\delta^{13}C$" equation for the Early Neolithic samples and the "EBA sites, $\delta^{13}C$ and $\delta^{15}N$" equation for Early Bronze Age samples. For individuals from the Angara River we have used Schulting et al.'s "SW Baikal/Angara²" Equation (2014, Table 4 pp. 998) that is based on their treating analyzed graves separately. Due to the fact that we are analyzing petrous bones and dentine, however, it should be noted that our reservoir estimates are best treated as 'maximum' estimates given the potential impact of the 'weaning effect' on $\delta^{13}C$ and $\delta^{15}N$, particularly on First Molars (Fuller et al., 2003) and even perhaps petrous bones (Jørkov et al., 2009).

The $\delta^{13}C$ and $\delta^{15}N$ results of the samples analyzed are shown in Table S1. The data is broadly consistent with individuals living in a predominantly C_3 environment and consuming significant amounts of freshwater resources (see also Katzenberg et al., 2010). There is a distinction between individuals excavated along the Lena and Angara Rivers, with the latter having higher $\delta^{13}C$ and $\delta^{15}N$ suggesting increasing amounts of freshwater resources in the diets of these individuals (Table S1). Katzenberg et al. (2010) reported Late Neolithic and Bronze Age human $\delta^{13}C$ of between -20 and -19 ‰ for the Lena and Angara Rivers, with $\delta^{15}N$ of c. 10.0 ‰. Our human data ($\delta^{13}C = c. -20$ to -16 ‰; $\delta^{15}N$ c. 10 to 16 ‰) is consistent with interpretations of a C_3-dominated diet, though with significantly varying, and often greater, contributions of freshwater fish to the diet relative to Katzenberg et al.'s dataset for the same region. While some of this difference is likely a product of the fact that one of the individuals with the highest $\delta^{13}C$ and $\delta^{15}N$ is dated to the Early Neolithic at Angara (where more fish consumption was also noted by Katzenberg et al., 2010), and another individual with highest $\delta^{13}C$ and $\delta^{15}N$ is represented by an M1 that is likely influenced by the breastfeeding effect, it is clear that even on a cross-tissue basis, freshwater resources may have resulted in radiocarbon offsets in a number of these individuals (Table S1). The calculated offsets are shown in Table S1, with individuals from the Lena River having offsets between 161 and 618 years (with many centering around 300 years) and those from the Angara River having offsets from between 246 and 485 years (with 3 of the 4 individuals centering around 400 years) (Table S1).

Strontium isotope analysis
Background

The use of strontium isotope ratios ($^{87}Sr/^{86}Sr$) to determine human mobility rests on the basic concept that rocks of different ages and compositions have distinctive values that do not fractionate from the bedrock into the biosphere (including the tissues of any individual measured) (Graustein and Armstrong, 1983; Montgomery, 2010). Older rocks have relatively higher $^{87}Sr/^{86}Sr$ when compared to younger rocks, while different mineral contents (with different $^{87}Sr/^{86}Sr$ ratios) leads to characteristic $^{87}Sr/^{86}Sr$ based on rock 'type' (Capo et al., 1998). For example limestones have lower Rb/Sr ratios than continental granites (Montgomery, 2010). While there is a

lack of mass-dependent fractionation from the bedrock into the foodchain, bedrock $^{87}Sr/^{86}Sr$ does not always correlate with bioavailable $^{87}Sr/^{86}Sr$. Differential weathering of rocks with different $^{87}Sr/^{86}Sr$ ratios, as well as the geographic variability of hydrology and aeolian transport, lead to variations in the $^{87}Sr/^{86}Sr$ of soils and plants overlying a given distribution of rocks (Montgomery, 2010).

From plants, Sr^{2+} actively replaces Ca^{2+} in consumer tissues as part of the process of nutrient uptake and excretion (Montgomery, 2010; Rokita et al., 1993), with the amount of strontium incorporated into the skeleton believed to be directly reflective of that available from the diet (and environment) (Montgomery, 2010; Price et al., 1986). In the context of tooth enamel from permanent teeth, Sr^{2+} (and $^{87}Sr/^{86}Sr$ ratios) will be incorporated during the process of mineralizaton which will vary depending on the tooth sampled anywhere between ten weeks before birth and 16 years of age (Hillson, 1996). By sampling teeth that form during different periods of life, and comparing the $^{87}Sr/^{86}Sr$ values of these teeth to bioavailable $^{87}Sr/^{86}Sr$ values in the burial locale of an individuals, it is possible to determine whether someone grew up in a different location to that in which they were buried, thus determining potential migration during the life of an individual (Bentley et al., 2003; Montgomery, 2010). Robustness and detail of the bioavailable baseline created is important as the $^{87}Sr/^{86}Sr$ of an individual will be the combined consequence of all food consumed and all water drunk, as well as the extent of the range over which it obtains food and drink (significant in the context of trade in food or presence of long rivers) (Montgomery, 2010), which can complicate interpretation.

Strontium isotope analysis

We sampled a total of 11 human teeth (Table S1) from the Angara River Valley (GLZ001, GLZ002, GLZ003, ANG001) and the broader Baikal region (KAG002, KPT002-KPT006, ZPL002) for strontium isotope analysis. The teeth sampled were permanent 1st, 2nd and 3rd molars, which represent different periods of life (0-3 years, 3-7 years and adult respectively as per Alexander Bentley, 2006), to see if there were any distinctions between their $^{87}Sr/^{86}Sr$ ratios during childhood and the bioavailable $^{87}Sr/^{86}Sr$ of their burial location. We used the comprehensive dataset of Haverkort et al. (2010) that includes modern and archaeological fauna from terrestrial and aquatic settings as an indication of the local baseline.

For each tooth, adhering sediments were removed and teeth were cleaned ultrasonically in ultra-pure water (deionized water). Teeth were then air-dried overnight and a groove was made along the buccal edge of the tooth, in order to average the signal for the period of enamel formation (Alexander Bentley, 2006), using a Dremel drill at the Stable Isotope Laboratory of the Department of Archaeology, Max Planck Institute for the Science of Human History, Jena, Germany.

Drill powdered samples of 20 mg were then shipped to the clean laboratory in the Department of Geological Sciences at the University of Cape Town. Samples were dissolved in 2 mL 65% 2B HNO_3 in a closed Teflon beaker and placed for one hour on a hotplate at 140°C. The samples were then dried down and re-dissolved in 1.5 mL 2 M HNO_3. Strontium separation chemistry followed methods discussed in Pin et al. (1994). After separation, the solutions for each sample were dried, dissolved in 2 mL 0.2% HNO_3 and diluted to 200 ppb Sr concentrations for strontium isotope analysis. Radiogenic $^{87}Sr/^{86}Sr$ ratios were measured using a Nu Instruments NuPlasma HR MC-ICP-MS in the Department of Geological Sciences at the University of Cape Town. Sample values were corrected for instrumental mass fractionation using an $^{86}Sr/^{88}Sr$ ratio of 0.1194 (Nier, 1938) and isobaric ^{87}Rb interference using the measured ^{85}Rb signal and natural Rb isotope ratios. All data presented are referenced to bracketing analyses of NIST SRM987 ($^{87}Sr/^{86}Sr$ reference value of 0.710255). Results for repeat analyses of an in-house carbonate standard (NM95) processed and measured with the batches of unknown samples in this study gave an $^{87}Sr/^{86}Sr$ ratio of 0.708885 ($2\sigma = 0.000010$; $n = 40$) are in agreement with long-term results for this in-house standard having an average $^{87}Sr/^{86}Sr$ ratio of 0.708911 ($2\sigma = 0.000040$; $n = 414$).

Ancient DNA processing

All samples were processed in dedicated laboratories at the Max Planck Institute for the Science of Human History in Jena, Germany, except the single-stranded library of sample UKY001.B that was generated at the Max Planck Institute for Evolutionary Anthropology in Leipzig, Germany. Bone powder for DNA extraction was obtained from petrous bones by drilling the densest osseous matter around the cochlea, and from teeth by cutting at the junction between the root and crown, sampling the dental pulp. The sample UKY001 was already fragmented and two fragments were milled using the MM200 mixer mill (Retsch). The resulting bone powder was split in three equal aliquots. For detailed information on the analyzed samples, their archaeological context and radiocarbon age see Table S1 and STAR Methods.

DNA from the 19 ancient individuals was extracted following established protocols (Dabney et al., 2013). The sample UKY001.B was pre-treated with a washing step to reduce surface contamination (Korlević et al., 2015). A negative and cave bear positive controls were included. To release DNA from 30–100 mg of bone powder, a solution of 900 μL EDTA, 75 μL H2O and 25 μL Proteinase K was added. In a rotator, samples were digested for at least 16 h at 37°C, for UKY001.B this was followed by an additional hour at 56°C (Rohland and Hofreiter, 2007). The suspension was then centrifuged and transferred into a binding buffer as previously described (Dabney et al., 2013). To bind DNA, silica columns for high volumes (High Pure Viral Nucleic Acid Large Volume Kit; Roche) were used. After two washing steps using the manufacturer's wash buffer, DNA was eluted in TET (10 mM Tris, 1 mM EDTA and 0.05% Tween) in two steps for a final volume of 100 μl.

Double-stranded DNA libraries were built from 25 μL of DNA extract in the presence of uracil DNA glycosylase, following a double-stranded 'UDG-half' library preparation to reduce, but not eliminate, the amount of deamination-induced damage toward the ends of ancient DNA (aDNA) fragments (Rohland et al., 2015). Negative and positive controls were carried alongside each experiment. Libraries were quantified using the IS7 and IS8 primers (Meyer and Kircher, 2010) in a quantification assay using a DyNAmo SYBP Green qPCR Kit (Thermo Fisher Scientific) on the LightCycler 480 (Roche). Each aDNA library was double indexed (Kircher et al.,

2012) in 1–4 parallel 100 μl reactions using PfuTurbo DNA Polymerase (Agilent). The indexed products for each library were pooled, purified over MinElute columns (QIAGEN), eluted in 50 μL TET and again quantified using the IS5 and IS6 primers (Meyer and Kircher, 2010) using the quantification method described above. 4 μl of the purified product were amplified in multiple 100 μL reactions using Herculase II Fusion DNA Polymerase (Agilent) following the manufacturer's specifications with 0.3 μM of the IS5/IS6 primers. After another MinElute purification, the product was quantified using the Agilent 2100 Bioanalyzer DNA 1000 chip. An equimolar pool of all libraries was then prepared for shotgun sequencing on Illumina Hiseq4000 platform using 75bp single-end reads for screening.

The single-stranded DNA library for sample UKY001.B was built from 30 μL of DNA extract in the absence of uracil DNA glycosy-lase (non-UDG library) followed by double indexing, using an automated version of the protocols described in Gansauge et al. (2017) and Kircher et al. (2012) on a liquid handling system (Agilent Technologies Bravo NGS Workstation).

Human genome enrichment and sequencing

Both double-stranded UDG-half and single-stranded non-UDG-treated libraries were further amplified with IS5/IS6 primers to reach a concentration of 200–400 ng μl–1 as measured on a NanoDrop spectrophotometer (Thermo Fisher Scientific). Mitochondrial DNA capture (Fu et al., 2013) was performed on screened double-stranded libraries, after shotgun sequencing, showed the presence of aDNA, highlighted by the typical C-to-T and G-to-A substitution pattern toward 5′ and 3′ molecule ends, respectively (Table S1). Eight of the libraries with percentages of human DNA over 10% were deep shotgun sequenced on an Illumina HiSeq 4000 instrument with 75 pair-end-run cycles using the manufacturer's protocol. Furthermore, samples with a percentage of human DNA in shotgun data around 0.1% or greater were enriched for a set of 1,237,207 targeted SNPs (1240K capture) across the human genome (Fu et al., 2015). The enriched DNA product was sequenced on an Illumina HiSeq 4000 instrument with 75 single-end-run cycles using the man-ufacturer's protocol.

The de-multiplexed capture sequencing reads were cleaned and mapped to human reference genome hs37d5 using EAGER pipe-line 1.92.55 (Peltzer et al., 2016). Within the pipeline, the adapters were removed by AdapterRemoval 2.2.0 (Schubert et al., 2016), reads were mapped with BWA 0.7.12 aln/samse algorithm (Li and Durbin, 2009), duplications were removed by DeDup 0.12.1 (https://github.com/apeltzer/DeDup) and damage patterns of each library were checked with mapDamage 2.0.6 (Jónsson et al., 2013). Then we masked 2bp from both ends of the reads from double-stranded libraries with trimBam in bamUtil 1.0.13 (https://github.com/statgen/bamUtil) to remove the damaged sites.

The mitochondrial capture sequencing reads were cleaned by AdapterRemoval 2.2.0 to remove the adapters. Then the cleaned reads were mapped to human reference mitochondrial sequence GenBank: NC_012920.1 with BWA 0.7.12 aln/samse algorithm and realigned with CircularMapper (Peltzer et al., 2016). After removing duplication with DeDup, the consensus sequences were generated by Schmutzi (Renaud et al., 2015).

Y. pestis genome enrichment

Samples GLZ001 and GLZ002 that were putatively positive for *Y. pestis* were also converted into Illumina double-stranded libraries with 50 μL of input DNA extract. As post-mortem aDNA cytosine deamination can influence read mapping and SNP identification, we used an initial uracil-DNA-glycosylase (UDG) and endonuclease VIII treatment (USER enzyme, New England Biolabs) for uracil exci-sion and subsequent DNA repair (Briggs et al., 2010). The rest of the library preparation steps were proceeded with according to a published protocol (Meyer and Kircher, 2010). Subsequently, the primer combination IS7/IS8 was used to quantify the resulting li-braries using a qPCR (Roche). For a double-indexing step (Kircher et al., 2012), each library was assigned a unique combination of indexing primers (each primer containing a unique 8bp identifier), and was split into multiple PCR reactions based on the initial quantification (IS7/IS8) so that each indexing reaction does not exceed 2×10^{10} input DNA copies. The indexing PCR reaction was carried out for 10-cycles using the enzyme Pfu Turbo Cx Hotstart DNA Polymerase (Agilent). Reaction products were cleaned up using the MinElute DNA purification kit (QIAGEN), eluted in TET (10mM Tris-HCl, 1mM EDTA pH 8.0, 0.05% Tween20), and quan-tified using a qPCR (Roche) with the IS5/IS6 primer combination (Meyer and Kircher, 2010). Moreover, indexed libraries were ampli-fied using the enzyme Herculase II Fusion DNA Polymerase (Agilent) to achieve 1-2 μg of total DNA in 7 μl, which would be used as input for whole-genome *Y. pestis* enrichment. PCR products were purified with the MinElute DNA purification kit (QIAGEN) and eluted in EBT (QIAGEN EB, 0.05% Tween20). In-solution *Y. pestis* captures of both full-UDG and partially-UDG-treated libraries were per-formed using a published protocol (Fu et al., 2013), adapted for *Y. pestis* as described previously (Andrades Valtueña et al., 2017).

QUANTIFICATION AND STATISTICAL ANALYSIS

Genotyping and dataset preparation for analysis

The cleaned reads with base quality and mapping quality over 30 were piled up with mpileup in SAMtools 1.3 (Li et al., 2009). For double-stranded libraries, we called pseudo-haploid genotypes with pileupCaller 1.2.2 (https://github.com/stschiff/sequenceTools) under random haploid calling mode. For the single-stranded library UKY001.B0102, we called pseudo-haploid ge-notypes with pileupCaller 1.4.0.3 under single-strand mode using both shotgun and capture sequencing reads, which ignores for-ward reads at C/T polymorphisms and reverse reads at G/A polymorphisms. Then we combined our genotypes with published ancient individuals (Allentoft et al., 2015; Damgaard et al., 2018b, 2018a; Flegontov et al., 2019; Jeong et al., 2018, 2019; Jones et al., 2015; Lazaridis et al., 2016; Mathieson et al., 2015; Moreno-Mayar et al., 2018; Olalde et al., 2018; Rasmussen et al., 2010,

2014, 2015a; Saag et al., 2017; Scheib et al., 2018; Sikora et al., 2019; Siska et al., 2017) and further intersected the dataset with Affymetrix Axiom Human Origins array SNPs in order to compare with worldwide modern populations. This final dataset of 539,124 SNPs on autosomes is used for downstream population analysis.

With shotgun sequencing reads of base quality over 30, we individually calculated the genotype likelihood on 27.9 million bi-allelic SNPs with minor allele count 5 or higher published in the 1000 Genomes Project Phase 3 dataset (Auton et al., 2015), using GATK UnifiedGenotyper 3.5 (DePristo et al., 2011). For half-UDG-treated double-stranded libraries, we used 2bp-trimmed reads for genotype likelihood calculation. For the single-stranded library, we ignored forward reads at C/T polymorphisms and reverse reads at G/A polymorphisms. For non-UDG-treated libraries of published ancient individuals from the Lake Baikal region (Damgaard et al., 2018a; Sikora et al., 2019), we only calculated the genotype likelihood on transversion sites.

Then we applied GeneImp 1.4 (Spiliopoulou et al., 2017) to impute diploid genotypes on the 1000 Genomes Phase 3 variations, with the genotype likelihood as input and the 2504 individuals in 1000 Genomes Phase 3 as reference. Following the developer's guideline in the original publication, we ran imputations with three different window sizes, kl = 15, 20 and 25 and took the average GP (genotype call probabilities) as posterior probability for each imputed genotype.

Then all the genotypes with posterior probability of 0.99 or higher were extracted and 24 individuals with genotyping rate over 75% were included in downstream analysis (Table S1), including one Upper Paleolithic UKY individual, one Mesolithic Kolyma individual, 12 Early Neolithic individuals and 10 Late Neolithic to Bronze Age individuals. We intersected the imputed SNPs with 1240K and HumanOrigins array SNPs, and kept 520,289 sites with over 50% genotyping rate in our 24 individuals for downstream phasing.

For the IBD analysis that requires phased genotype data, we jointly phased the 24 imputed individuals with 3014 worldwide modern individuals (Table S1) using SHAPEIT v2.r837 (Delaneau et al., 2013), with a genetic map from 1000 Genomes Phase 3 data, under its default settings.

The sex of each individual was determined by coverage on sex chromosomes (Table S1). Then Y chromosome haplogroups of male individuals were determined by yHaplo program (Poznik, 2016).

The nuclear DNA contamination of male individuals was estimated by ANGSD 0.910 (Korneliussen et al., 2014) based on mismatch rate on the X chromosome. For the single-stranded library without UDG-treatment, we kept only transversion sites for the estimation. The mitochondrial DNA contamination was estimated by schmutzi (Renaud et al., 2015).

Population genetics analysis

The principal component analysis was carried out by smartpca in EIGENSOFT 6.0.1 (Patterson et al., 2006), with modern individuals used for calculation and all the ancient individuals projected on the calculated PCs. The "lsqproject: YES" parameter was used to minimize the effect of missing data in ancient individuals. The PCA was calculated with 2182 individuals from 181 Eurasian and Native American modern populations (Figure 1C; Table S1).

The unsupervised population clustering pattern was estimated by ADMIXTURE 1.3.0 (Alexander et al., 2009). We included 3488 individuals in the ADMIXTURE analysis, including 2986 worldwide modern individuals, 483 selected ancient individuals and 19 individuals newly genotyped in this study. Before ADMIXTURE analysis, the dataset was filtered to 120,599 SNPs with PLINK 1.90 (Purcell et al., 2007) to remove SNPs with minor allele frequency lower than 0.01 (–maf 0.01) and linked SNPs with $r^2 > 0.2$ (–indep-pairwise 200 25 0.2). The ADMIXTURE analysis was carried out with population number (K) from 2 to 20, five duplications for each K value and we chose K = 16 as it gave the lowest cross-validation (CV) error.

We identified the ROH and shared IBD segments in the 24 shotgun sequenced individuals and 81 individuals from several modern Siberian populations (Buryat, Even, Evenk_FarEast, Evenk_Transbaikal, Nganasan, see Table S1). The 24 ancient individuals are divided into four groups, namely UKY, Kolyma, Baikal EN and Baikal LNBA (Table S1). The ROH was detected using PLINK v1.90b3.29 (Purcell et al., 2007), with the "–homozyg" flag and default settings. The shared IBD segments between individuals were detected using Refined IBD algorithm in BEAGLE v4.1 (Browning and Browning, 2013), under the default parameter settings with the HapMap GRCh37 genetic map provided by BEAGLE (http://bochet.gcc.biostat.washington.edu/beagle/genetic_maps/).

The f_3 statistics was calculated with qp3Pop 435 in ADMIXTOOLS 5.1 package (Patterson et al., 2012), and the f_4 statistics was calculated by qpDstat 755 with parameter "f4 mode: YES." The Mbuti population from Africa was used as outgroup in all f-statistics analysis.

Admixture modeling with qpAdm

The qpAdm 810 in ADMIXTOOLS 5.1 was applied to model the ancestries of admixed populations. We chose an outgroup set of seven populations (stdright), including modern African Mbuti (n = 10), Paleolithic European Villabruna (n = 1), Levantine hunter-gather Natufian (n = 6), Neolithic Iranian farmer Iran_N (n = 5), modern South Asian Onge (n = 11), Southeast Asian Ami (n = 10) and Native American Karitiana (n = 16), to distinguish ancestries across Eurasian continent. For the modeling of KPT005 with possible West Eurasian ancestry, we also included Neolithic Anatolian farmer Anatolia_N (n = 25) in the outgroup (stdright_Anatolia) in order to distinguish the Yamnaya-related and Sintashta-related ancestries. Before running qpAdm, all the reference combinations were tested by qpWave 410, to make sure the outgroup set could distinguish all sources (Table S3).

Demographic modeling with *qpGraph*

We used *qpGraph* 6450 to reconstruct a demographic model of studied populations. For the resolution of graphic modeling, we applied "useallsnps" mode to correct for low-coverage sample and carried out this part of analysis using 1240K SNP dataset. Starting from (Mbuti, (AG3, Onge)), we first iteratively added the Devil's Gate, USR1, Ancient Southwestern Ontario (ASO, n = 6) and Early San Nicolas (ESN, n = 17) to build a skeleton graph based on previous publications (Posth et al., 2018), with USR1, ASO and ESN forming a single group which is the mixture of AG3 and Devil's Gate, and USR1 outgroup to ASO and ESN.

Then we added UKY and Kolyma independently to this graph, considering them as either sister lineage of existing node, or two-way admixture of the existing lineages. For each population, we tested 91 different models and chose the best fitted model based on the worst Z scores and the final likelihood scores reported by each model. After obtaining the best fitted model with UKY or Kolyma (Figure S2), we further tested 340 different models by adding Kolyma onto the best UKY model, or vice versa, to find the best fitted graph including both of these individuals.

Admixture dating with *DATES*

We applied the ancestry covariance pattern-based *DATES* 753 program (Moorjani and Patterson, 2018) to estimate the time of admixture events in Lake Baikal and Okunevo populations. For the Baikal populations, we used a pooled population ANE_pool (n = 15, including MA1, AG2, AG3, EHG, Botai, West_Siberia_N) to represent the ANE-related ancestry, and population EA_pool (n = 39, including Devil's Gate, Ulchi and Nanai) to represent the NEA ancestry. For the Okunevo population, the three ancestries were represented by Baikal_LNBA_all (n = 34), Yamnaya_pool (n = 43, including Yamnaya_Samara, Yamnaya_Karagash, Yamnaya_Kalmkia and Afanasievo) and Botai_pool (n = 8, including Botai and West_Siberia_N), respectively. For the BZK002 individual, we used the same Baikal_LNBA_all and Botai_pool to represent the two ancestries. The bin size for covariance calculation was 0.1cM and exponential fitting started at d $\geq$ 0.5cM.

Pathogen DNA screening with HOPS

The Megan Alignment Tool (MALT version 0.4.0) (Vågene et al., 2018) was used within the pathogen screening pipeline HOPS (Hübler et al., 2019), for the assessment of pathogen DNA in all Lake Baikal specimens analyzed in this study. Pre-processed shotgun NGS reads were used as input for MALT, against a custom database of all NCBI RefSeq bacterial and viral assemblies marked as complete, as well as a selection of eukaryotic pathogen genomes and the human GRCh38 reference (RefSeq, November 2017). Genomes with description keywords such as "unknown" were removed from the database, retaining a total of 15,361 entries. MALT was run with an 85 minimum percentage identity filter (–minPercentIdentity), 1 for the minimum support filer (–minSupport), a top percentage parameter of 1 (–topPercent) and a semi-global alignment mode, with all other parameters remaining as default. The MALT output was filtered with MALTExtract (within HOPS) based on a predefined list of bacterial, viral and eukaryotic pathogen candidates, where assigned reads were evaluated based on different parameters such as their coverage distributions, their edit distance and their aDNA damage profiles.

Read processing, SNP calling and phylogenetic analysis of *Yersinia pestis*

All captured libraries were sequenced on an Illumina HiSeq4000 (2x76+8+8 cycles). Processing of de-multiplexed NGS reads was performed within the automated pipeline EAGER v1.92.55 (Peltzer et al., 2016). In brief, AdapterRemoval v2 (Schubert et al., 2016) was used for removing Illumina adapters and for read filtering based on sequencing quality (minimum base quality of 20) and length ($\geq$30 bp). Moreover, for partially-UDG-treated libraries, both ends of NGS reads were trimmed to remove remaining deaminated sites, and the resulting files were concatenated with pre-processed read data from full-UDG-treated libraries. Furthermore, BWA (Li and Durbin, 2009) was used for read mapping against the *Y. pestis* chromosomal reference genome (GenBank: NC_003143.1), using a –n parameter of 0.1 and -l 32. The identical parameters were also used for mapping against the plasmid reference sequences (GenBank: NC_003131.1, GenBank: NC_003134.1 and GenBank: NC_003132.1), where nucleotide positions 3,000 - 4,200 were masked in pPCP1 as they were previously shown to display homology with an expression vector present in laboratory reagents (Schuenemann et al., 2011). Subsequently, SAMtools was used to remove reads with mapping quality lower than 37 and MarkDuplicates was used to remove PCR duplicates (http://broadinstitute.github.io/picard/).

SNPs were called on the chromosomal *Y. pestis* mapped reads using the UnifiedGenotyper in GATK (DePristo et al., 2011). GLZ001 and GLZ002 were analyzed alongside a dataset of modern *Y. pestis* genomes (n = 233) (Cui et al., 2013; Eroshenko et al., 2017; Kislichkina et al., 2015, 2018a, 2018b; Kutyrev et al., 2018; Morelli et al., 2010; Zhgenti et al., 2015) (as listed in (Keller et al., 2019)). In addition, we included previously published historical *Y. pestis* genomes with $\geq$ 10-fold coverage (Bos et al., 2011, 2016; Feldman et al., 2016; Keller et al., 2019; Namouchi et al., 2018; Spyrou et al., 2016, 2019), and all previously published Late Neolithic and Bronze Age genomes with $\geq$ 3-fold coverage (Andrades Valtueña et al., 2017; Rasmussen et al., 2015b; Spyrou et al., 2018). Geographic isolation locations of genomes within the comparative dataset are as follows: China (CHN), United States of America (USA), Madagascar (MDG), India (IND), Myanmar (MNM), Congo (COG), Uganda (UGA), Mongolia (MNG), Nepal (NPL), Iran (IRN), Kazakhstan (KAZ), Kyrgyzstan (KGZ), Armenia (ARM), Georgia (GEO), Azerbaijan (AZE), Uzbekistan (UZB), Turkmenistan (TKM), Tajikistan (TJK), Russia (RUS), unspecified regions of the Former Soviet Union (FSU), Switzerland (CHE), Germany (DEU), Spain (ESP), France (FRA), United Kingdom (GBR), Netherlands (NLD), Norway (NOR), Lithuania (LTU), Croatia (CRO), Estonia (EST).

SNPs were called using the 'EMIT_ALL_SITES' option in GATK, which generated a call for every position in the chromosomal reference genome (CO92). Subsequently, a custom java tool, MultiVCFAnalyzer v0.85 (https://github.com/alexherbig/MultiVCFAnalyzer), was used to produce a SNP table of variant positions across the entire dataset, excluding previously defined non-core regions, as well as mRNAs, tRNAs and tmRNAs (Cui et al., 2013; Morelli et al., 2010). Variants were retained based on the following conditions: homozygous SNP positions were called with a minimum coverage of 3-fold and a minimum genotyping quality of 30. For heterozygous positions, SNPs were retained when at least 90% of reads supported the call. When none of the conditions were met, an "N" would be inserted in the respective genomic position. A total of 7,052 SNPs were identified in the present dataset. The SNP alignment produced by MultiVCFAnalyzer v0.85 was used as input for a maximum likelihood (ML) phylogeny with 99% partial deletion filter, which retained 4,368 SNP positions. ML trees were built using the program RAxML (version 8.2.9) (Stamatakis, 2014), under the Generalized Time Reversible (GTR) substitution model (Tavaré, 1986) (four gamma rate categories). 1,000 bootstrap replicates were used to determine node support.

BEAST v1.8 tip dating of GLZ001 and GLZ002

The program TempEst v1.5 (http://tree.bio.ed.ac.uk/software/tempest/) was used to assess of the temporal signal across previously published genomes and calibration points on the *Y. pestis* LNBA lineage (Andrades Valtueña et al., 2017; Rasmussen et al., 2015b), including the modern isolate 0.PE.2 Pestoides F (Garcia et al., 2007) as outgroup. All overlapping variant positions across this set of genomes were used for the analysis, retaining a total of 374 SNPs in the dataset. The resulting correlation coefficient (*r*) was 0.88 and R^2 was 0.78 when including the 0.PE2 outgroup and 0.98 and 0.97, respectively, for the LNBA lineage alone. Such result suggests a strong temporal signal in the dataset.

Subsequently, we used BEAST v1.8 (Drummond and Rambaut, 2007) to estimate the tip dates of GLZ001 and GLZ002, using published radiocarbon date ranges across the LNBA lineage as uniform priors (in years before the present) as follows: RISE509 (uniform prior: 4836–4625, tip date: 4729), RK1.001 (uniform prior: 4828–4622, tip date: 4720), GEN72 (uniform prior: 4833–4592, tip date: 4721), Gyvakarai1 (uniform prior: 4571–4422, tip date: 4485), Kunila2 (uniform prior: 4524–4290, tip date: 4427), 1343UnTal (uniform prior: 4346–4098, tip date: 4203), 6Post (uniform prior: 3957–3832, tip date: 3873), RT5 (uniform prior: 3868–3704, tip date: 3789), RISE505 (uniform prior: 3694–3575, tip date: 3635). The tip date of the 0.PE2 outgroup was set to 0 (present). The input date range for GLZ001 and GLZ002 was constrained to be between 5000 and 3500 years before the present, which spans the entire temporal range of the LNBA lineage, and the starting value tip date was set to 4250 (midpoint). The graphical user interface BEAUti v1.8 (Drummond and Rambaut, 2007) was used to set up multiple runs using the coalescent constant size and coalescent skyline tree priors in combination with both a strict and a lognormal relaxed clock model. In addition, a GTR substitution model with four gamma rate categories was used for all runs. All set-ups were run in BEAST v1.8 (Drummond and Rambaut, 2007) using two independent chains of 25,000,000 states each. After run completion, chains were combined using LogCombiner (Drummond and Rambaut, 2007) with 10% burn-in and were then inspected in Tracer v1.6 to ensure run convergence (http://tree.bio.ed.ac.uk/software/tracer/) with all ESS values being > 200. The resulting mean tip dates and HPD95% intervals produced for GLZ001 and GLZ002 across all runs were viewed and analyzed in Tracer v1.6 (http://tree.bio.ed.ac.uk/software/tracer/).

Assessment of *Y. pestis* gene profiles

In order to assess the gene profiles of GLZ001 and GLZ002, we computed the coverage across of 150 previously defended virulence-associated and evolutionary-determinant *Y. pestis* genes (Demeure et al., 2019; Zhou and Yang, 2009). For this, the two newly reconstructed genomes were comparatively assessed alongside previously published representatives of the LNBA lineage (RISE509, RK1001, GEN72, Gyvakarai1, Kunila2, 1343UnTal85, 6Postillionstrasse, RISE505), a Bronze Age isolate showing signatures of flea adaptation (RT5), historical *Y. pestis* genomes from the first and second plague pandemics (Altenerding 2148, London ES 8124/8291/11972), representatives of modern isolates (0.PE2 Pestoides F, 0.PE4 Microtus 91001, 1.ORI CO92), as well as a *Y. pseudotuberculosis* strain (IP31953). Raw pre-processed reads from all aforementioned datasets were mapped against the CO92 reference chromosome and plasmids using BWA (-n 0.1, -l 32), without the subsequent use of a mapping quality filter. The coverage across the defined gene regions was calculated using BEDTools (Quinlan and Hall, 2010). The computed coverages were plotted in the form of a heatmap using the ggplot2 package within R version 3.2.1 (R Development Core Team, 2008; Wickham, 2016). In addition, previously defined substitutions or InDels within functionally relevant genes were manually inspected in GLZ001 and GLZ002 using the program IGV (Thorvaldsdóttir et al., 2013). These were: a non-synonymous substitution defining the *pla* gene variant involved in within-host bacterial dissemination (Zimbler et al., 2015), pseudogenization mutations in genes PDE2, PDE3, *ureD* and a 30bp duplication in *rcsA* associated with *Y. pestis* flea-colonization (Sun et al., 2014), as well as a pseudogenization mutation in *flhD* associated with immune evasion (Minnich and Rohde, 2007).
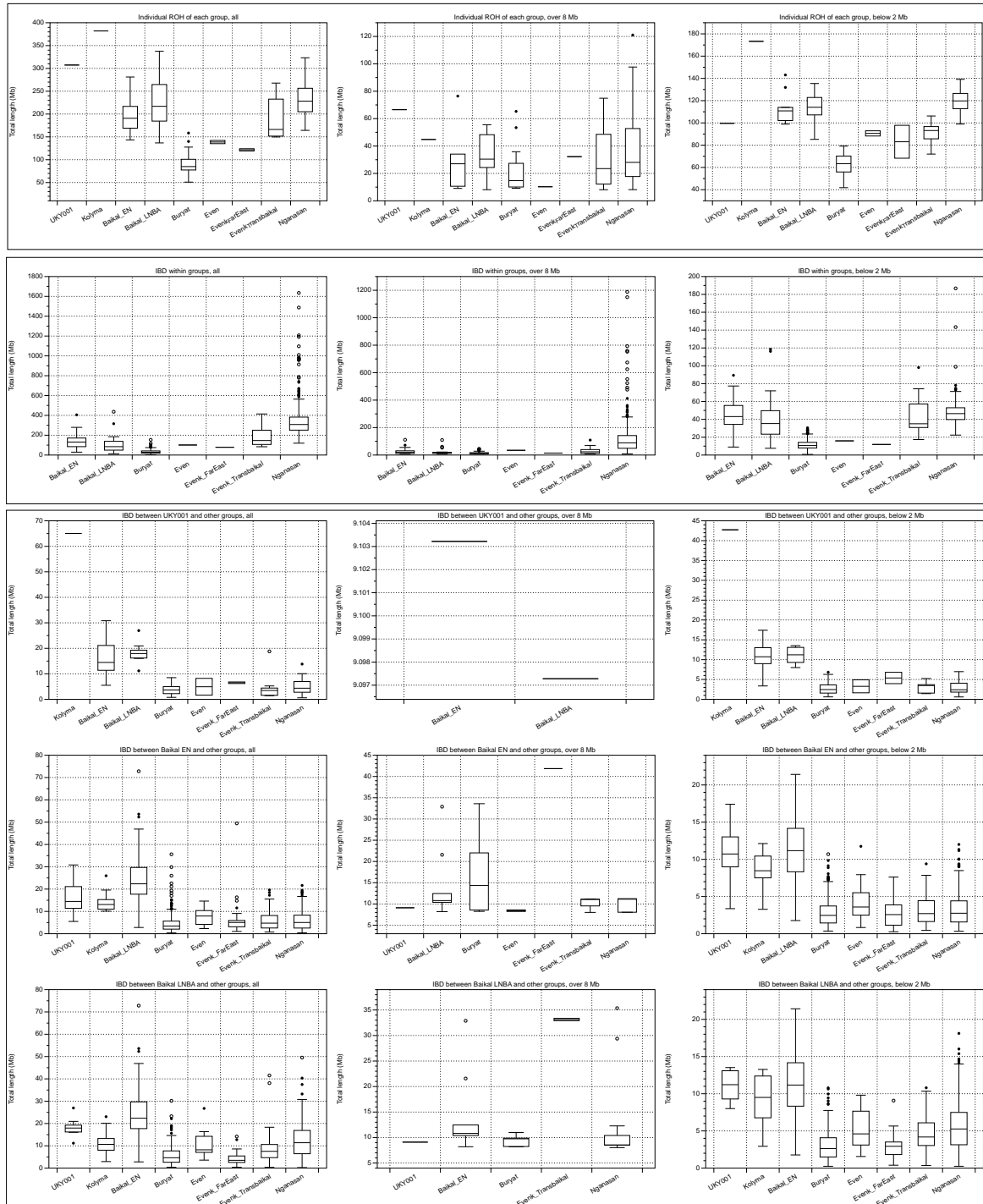
Supplemental Figures

Figure S1. Population Size and Relatedness of Lake Baikal Populations Revealed by ROH and IBD Segments, Related to Figure 1 and Table S1

This figure summarizes the accumulative ROH length detected in each individual (row 1), shared IBD segment length of individuals within population (row 2), and shared IBD segment length of UKY, Baikal_EN and Baikal_LNBA individuals with other population (row 3-5), respectively. The long segments (> 8Mb) and short segments (< 2Mb) are also summarized separately.
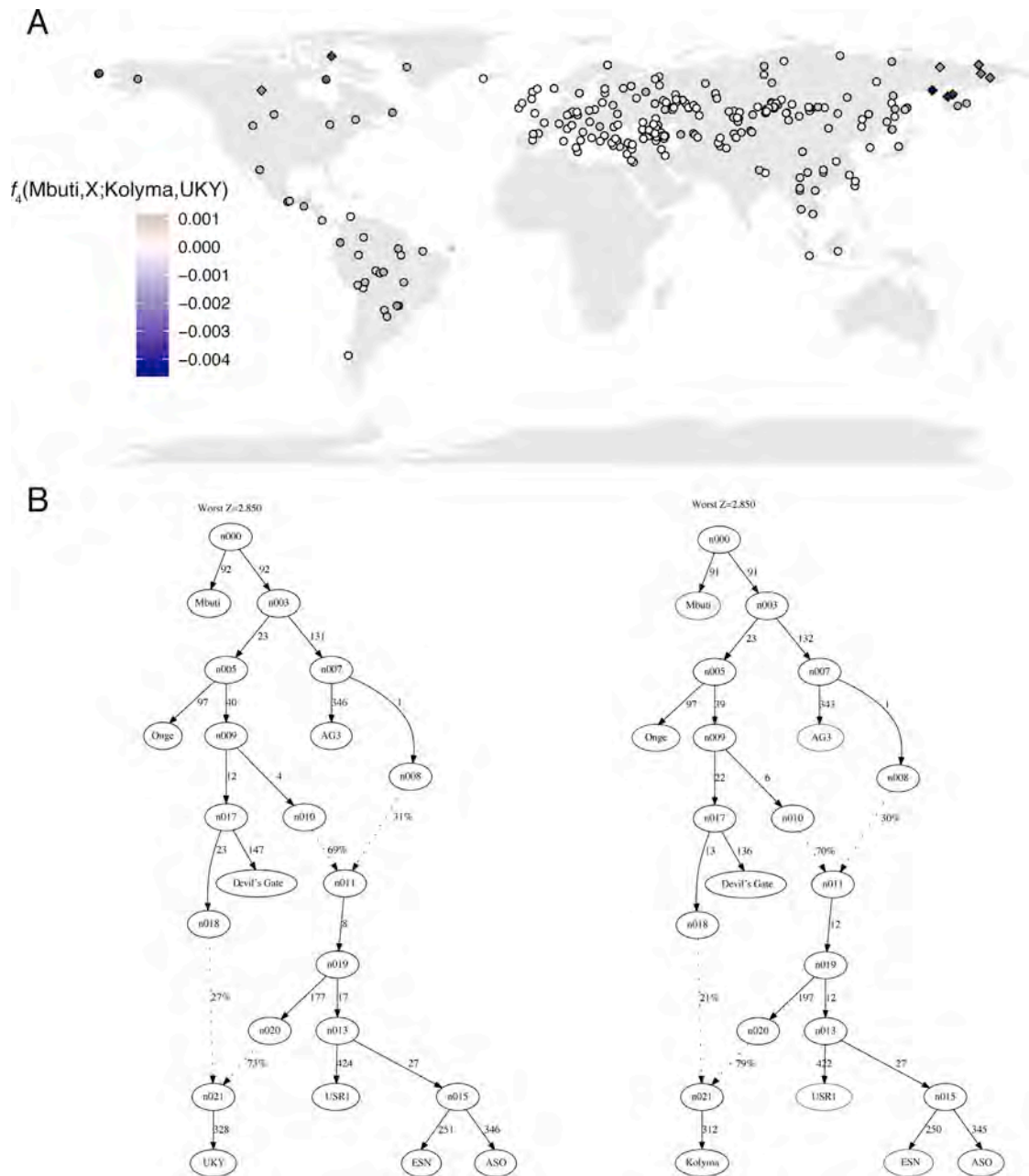
Figure S2. Relationship between UKY, Kolyma, and Modern-Day Populations Based on f_4 Statistics and *qpGraph* Modeling, Related to Figure 2

(A) This figure shows the different genetic affinities between UKY, Kolyma with worldwide population, assessed by f_4(Mbuti, X; Kolyma, UKY). The test populations with significant f_4 values (|Z| > 3) are shown in diamonds and other populations in circles.

(B) This figure shows the graphic modeling of UKY (left) and Kolyma (right) on the skeleton graph including Mbuti, AG3, Onge, Devil's Gate, USR1, ASO and ESN described in STAR Methods. The best fitted model for each individual is selected based on the maximum f-statistics Z scores and final scores reported for each model.
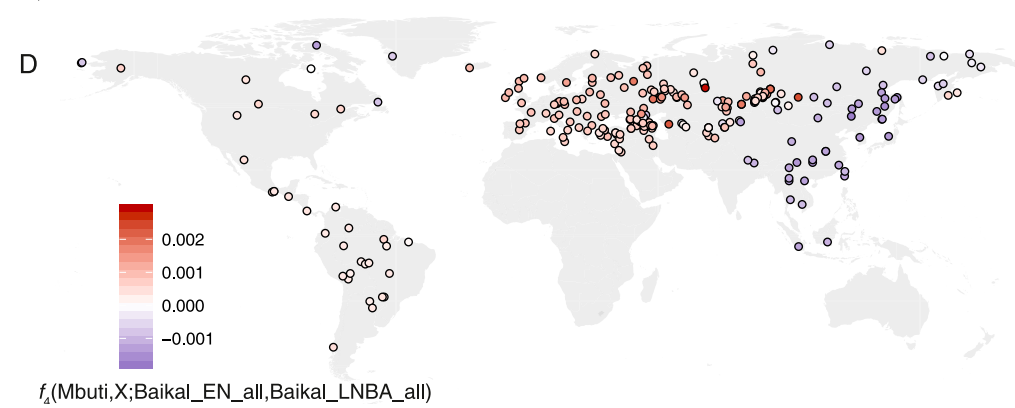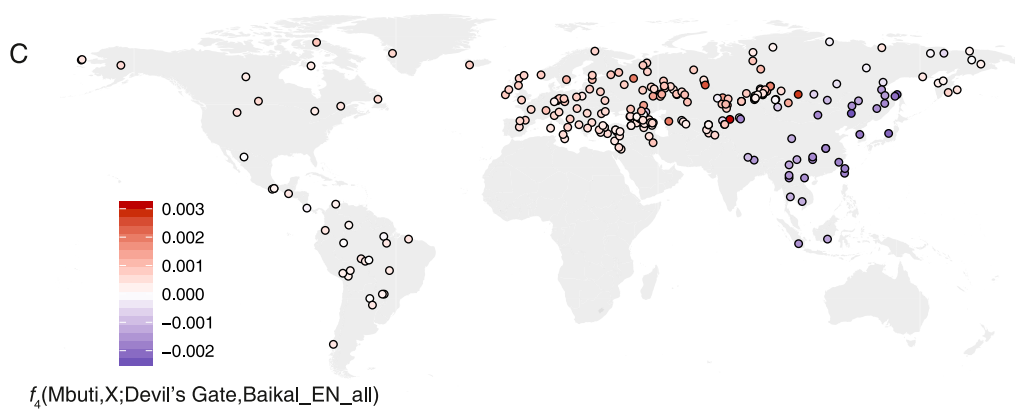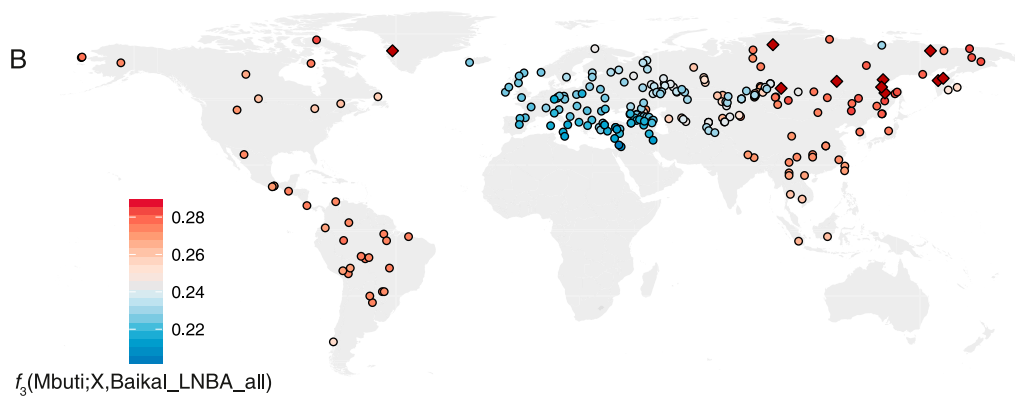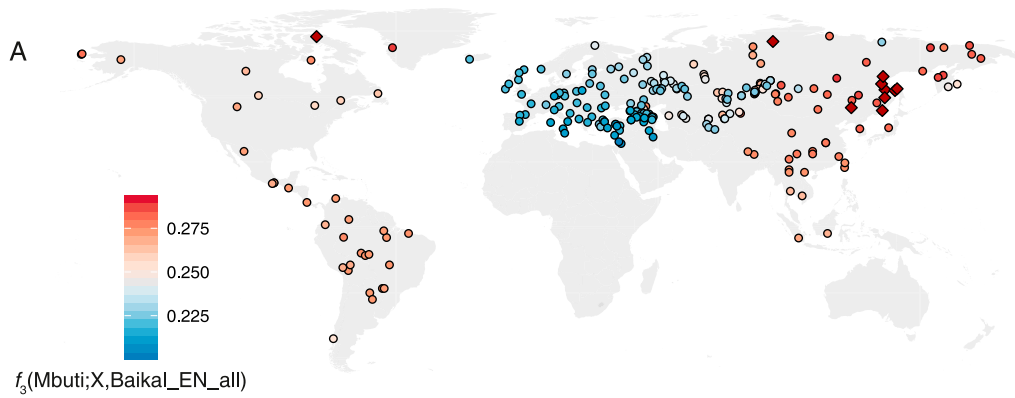
A

f_3(Mbuti;X,Baikal_EN_all)

B

f_3(Mbuti;X,Baikal_LNBA_all)

C

f_4(Mbuti,X;Devil's Gate,Baikal_EN_all)

D

f_4(Mbuti,X;Baikal_EN_all,Baikal_LNBA_all)
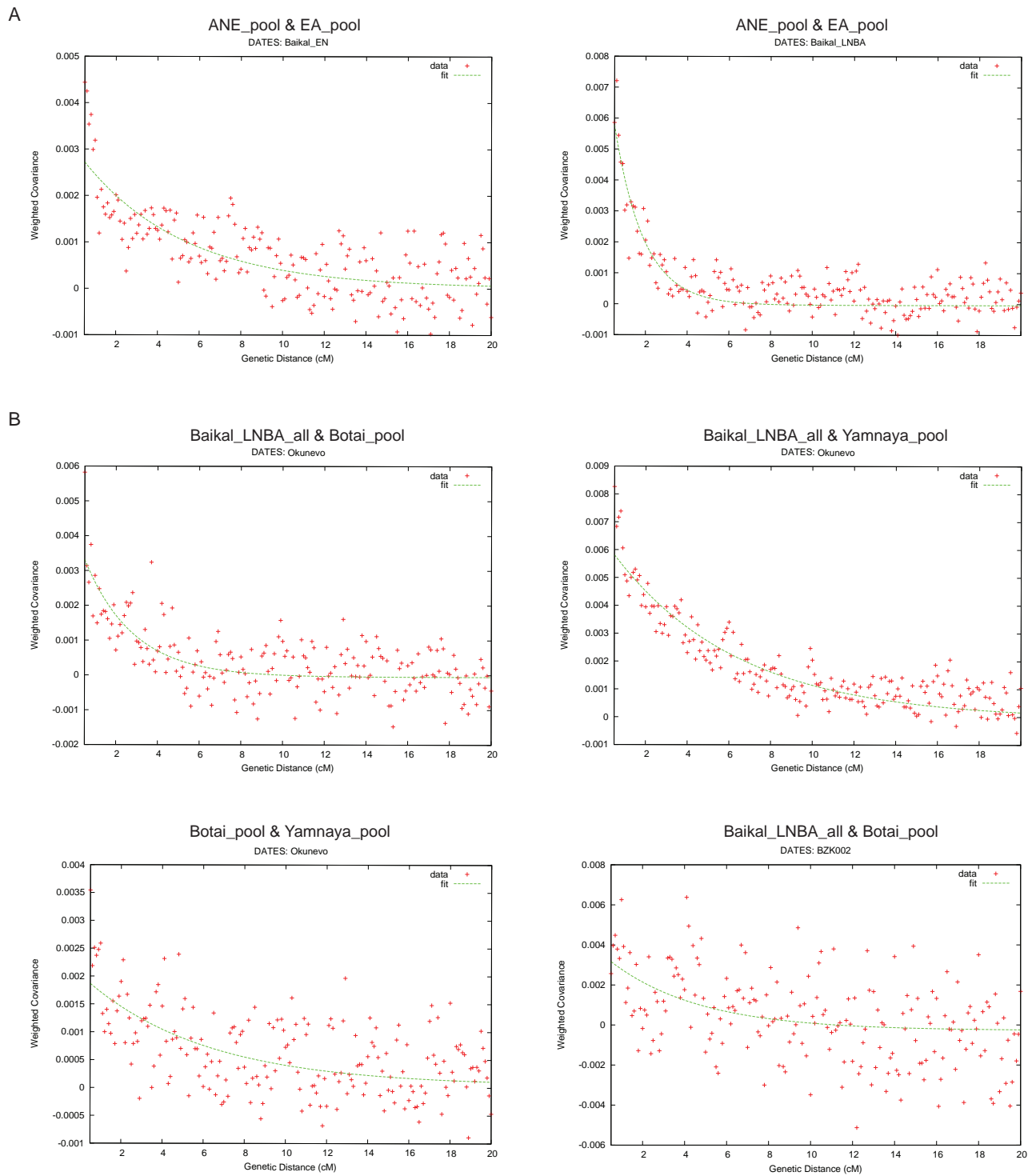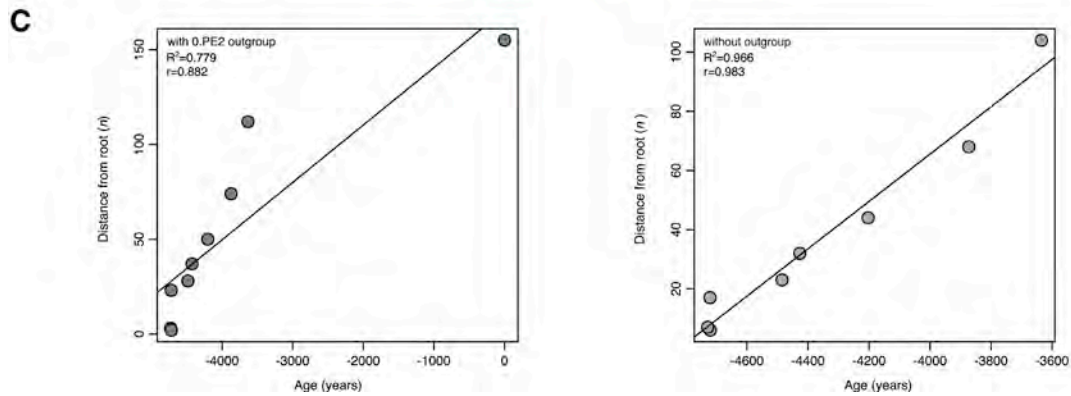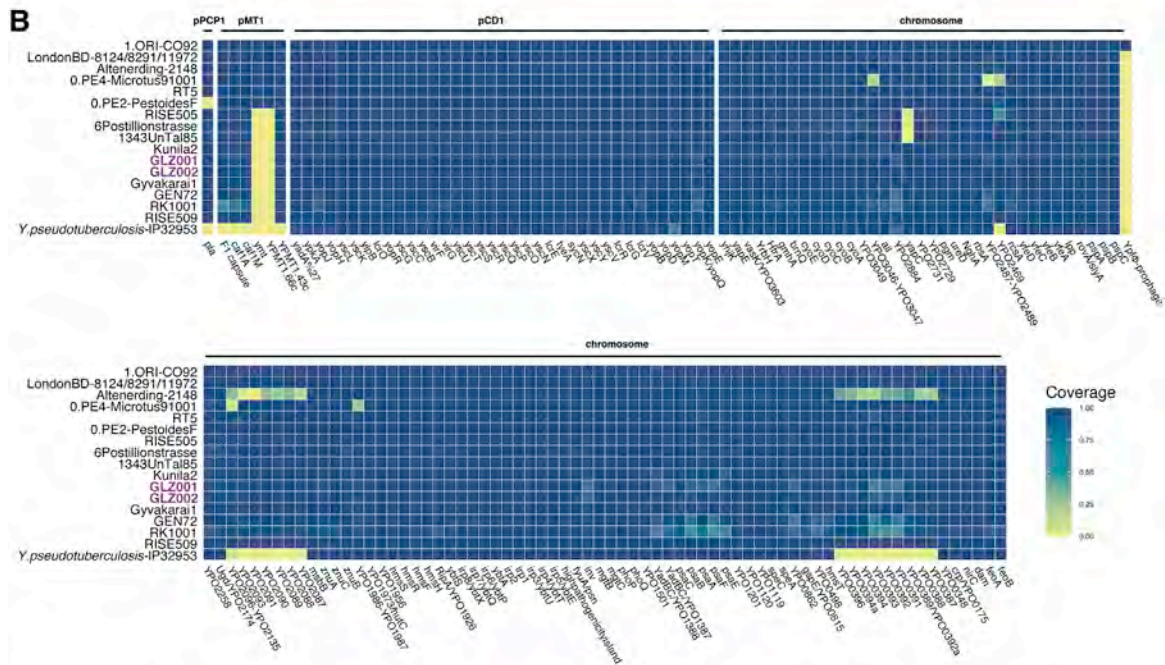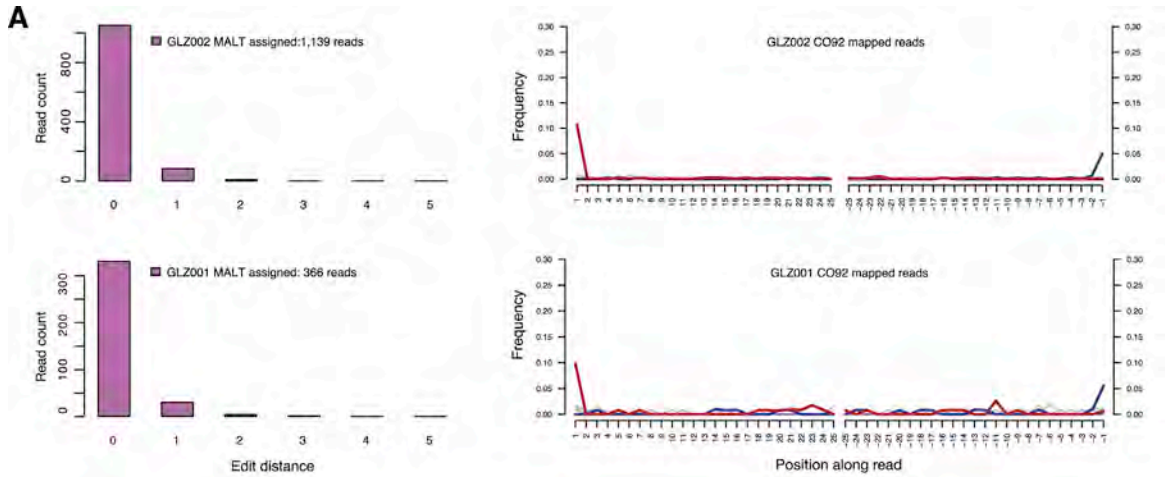
(legend on next page)

CellPress

Figure S4. Dating of the Admixture Events in Baikal, Okunevo Population, and the BZK002 Individual, Related to Figures 3 and 5 and Table S5

This figure shows the *DATES* estimation of (A) time of admixture events in Early Neolithic and LNBA Baikal population and (B) time of admixture events in Okunevo population and BZK002 with different ancestor pairs. The red cross dots show the weighted ancestry covariance in different genetic distances, and the green curves show the exponential fitting starting at 0.5 cM. Details of the results are listed in Table S5.

Figure S5. Overview of *Y. pestis* Screening, Gene Content, and Temporal Signal, Related to Figures 4 and S6 and Tables S1 and S6

(A) *Y. pestis* screening results for samples GLZ001 and GLZ002. The histograms were calculated in HOPS and represent the edit distance of GLZ001 and GLZ002 MALT assigned reads to their closest matching reference within the *Y. pseudotuberculosis* complex. In addition, aDNA damage patterns were generated using MapDamage2.0, after BWA mapping of all reads against the *Y. pestis* reference genome CO92.

(B) Presence/absence analysis of virulence-associated and evolutionary-determinant genes across *Y. pestis* genomes. The genomic profiles of GLZ001 and GLZ002 were investigated by calculating the coverage across virulence-associated and evolutionary-determinant genes, in comparison to those from previously published ancient strains from the LNBA period (RISE509, RK1001, GEN72, Gyvakarai1, Kunila2, 1343UnTal85, 6Postillionstrasse, RISE505), the Late Bronze Age (RT5), as well as from the medieval and early modern periods (Altenerding 2148 and London BD 8124/8291/11972). In addition, representatives of modern lineages were also included for comparative purposes. The investigated genes were located on the *Y. pestis* chromosome and the pMT1, pPCP1 and pCD1 plasmids. The heatmap was constructed in R version 3.2.1 using the ggplot2 package.

(C) Calculating the temporal signal within the *Y. pestis* LNBA lineage. Regressions of root-to-tip genetic distance against specimen age were calculated using TempEst v1.5 for all published LNBA genomes using a maximum likelihood phylogeny of 374 overlapping variant positions for the analysis. The input ages were as follows: RISE509 (4729 BP), RK.001 (4720 BP), GEN72 (4721 BP), Gyvakarai1 (4485 BP), Kunila2 (4427 BP), 1343UnTal (4203 BP), 6Post (3873 BP) and RISE505 (3635 BP). The left plot represents a linear regression of root-to-tip genetic distance against specimen age including a modern *Y. pestis* genome as outgroup (0.PE2 Pestoides F), whereas the right panel represents the regression including only previously published ancient genomes within the LNBA lineage (without the outgroup).
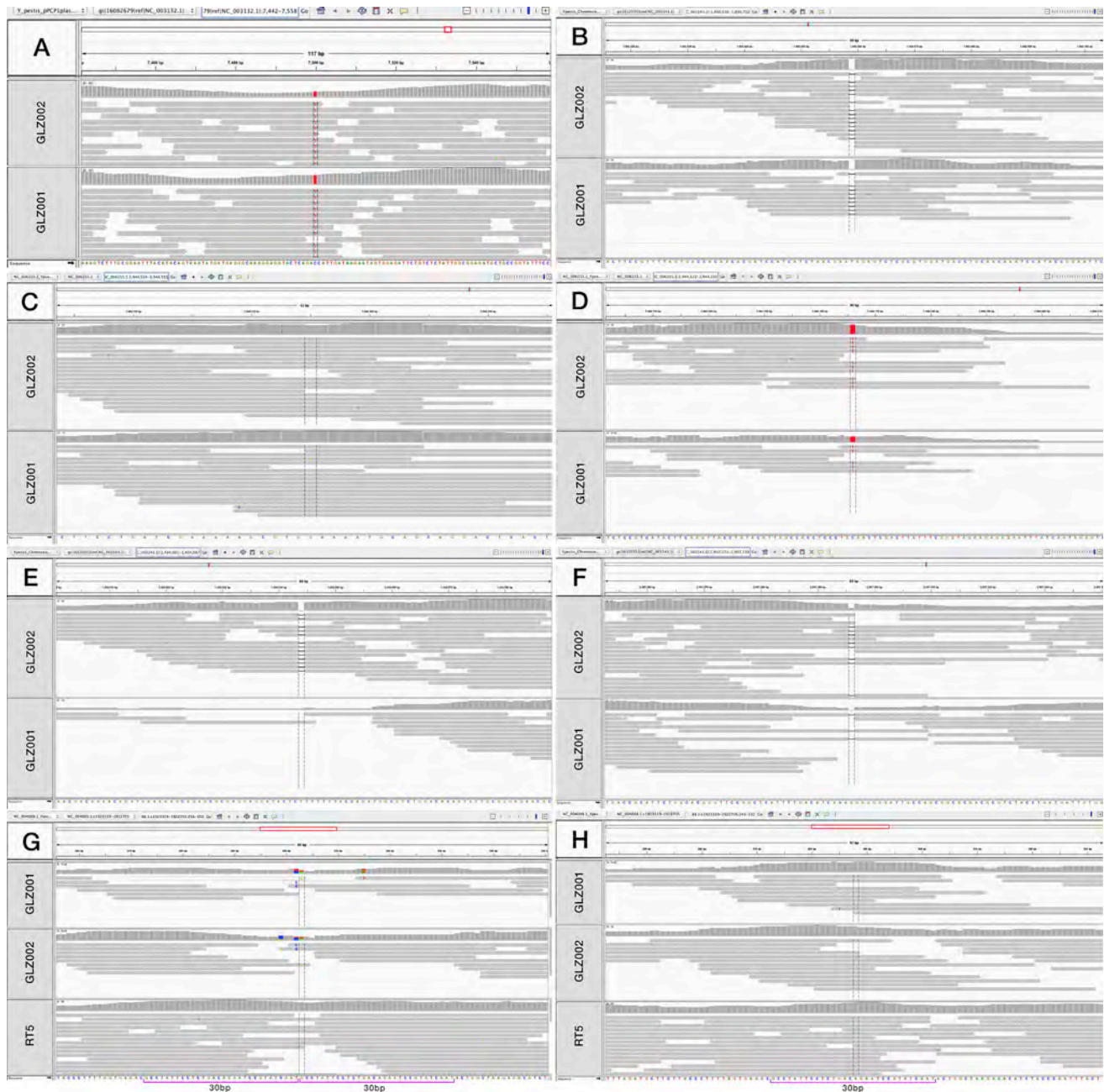
Figure S6. Visual Inspection of Functionally Informative *Y. pestis* SNPs in Virulence-Associated and Evolutionary-Determinant Genes, Related to Figures 4 and S5

Screenshots created in IGV (Thorvaldsdóttir et al., 2013) for a virtualisation of virulence-associated genes affected by substitutions or InDels. Visualized genomic positions are as follows: (A) presence of a "T" at CO92 pPCP1 plasmid position 7500 suggests ancestral *pla* variant; (B) lack of "T" insertion at CO92 chromosomal position 1892659 suggest active *flhD* gene variant; (C) Presence of "G" at chromosomal *Y. pseudotuberculosis* IP32953 position 3944534 suggests ancestral (active) PDE-3 variant; (D) presence of "T" at chromosomal *Y. pseudotuberculosis* IP32953 position 3944166 suggests derived (pseudogenised) PDE-3-pe'variant; (E) lack of "T" insertion at CO92 chromosomal position 1434044 suggests active PDE-2 variant; (F) lack of "G" insertion at CO92 chromosomal position 2997296 suggests active *ureD* variant; (G) imprecise mappability of reads spanning a 30bp duplication within *rscA* gene in GLZ001 and GLZ002 (mapped against the *rscA* [y1741] gene in KIM10), compared to the published ancient strain RT5 showing genetic evidence of flea adaptation (Spyrou et al., 2018); (H) exclusion of one 30bp duplicate from a constructed *rscA* reference restores read mappability within this region in GLZ001 and GLZ002, suggesting an absence of the duplication in those genomes.